NASA TECHNICAL NOTE

NASA TN D-3840

NASA TN D-3840

MAPPING A TUNGSTEN-REACTOR ROCKET ENGINE AS A GUIDE TO OPERATION AND CONTROL

by Richard H. Cavicchi

Lewis Research Center

Cleveland, Ohio

NATIONAL AERONAUTICS AND SPACE ADMINISTRATION • WASHINGTON, D. C. • MAY 1967

NASA TN D-3840

MAPPING A TUNGSTEN-REACTOR ROCKET ENGINE AS A GUIDE TO OPERATION AND CONTROL

By Richard H. Cavicchi

Lewis Research Center
Cleveland, Ohio

NATIONAL AERONAUTICS AND SPACE ADMINISTRATION

For sale by the Clearinghouse for Federal Scientific and Technical Information
Springfield, Virginia 22151 – CFSTI price $3.00

CONTENTS

MAPPING A TUNGSTEN-REACTOR ROCKET ENGINE AS A GUIDE TO OPERATION AND CONTROL

by Richard H. Cavicchi

Lewis Research Center

SUMMARY

A nonlinear analog simulation of a preliminary tungsten water-moderated reactor system indicated stability without external feedback controls. The simulation was used to obtain steady-state operating maps over a mass-flow range from 20 to 120 percent. A feasible operating corridor, outlined by locating system constraints on the maps, is bounded by the bleed-pump turbine speed limit at about 118 percent power and by bleed-pump stall at 33 percent power. Within this corridor, system operation is confined to a 500° R range in chamber temperature by heat-exchanger icing and the nozzle-wall temperature limit.

The manner of operating the bleed system determined the locations of the constraints on the maps except for the nozzle-wall and fuel-temperature limits. As chamber temperature was increased, temperature limits in the nozzle-wall, fuel, water-pump turbine-inlet, and pressure-tube were reached successively. Design specific impulse was potentially obtainable above 37 percent power, but the margin from the nozzle-wall temperature limit was small.

Reactor power could be controlled by the topping-turbine bypass valve and poison reactivity. Also, water temperature was a suitable control parameter. Reactor power was approximately proportional to hydrogen flow rate. A 10-cent insertion of poison reactivity reduced reactor power by about 7 percent; whereas less than a 3 percent change in power was accompanied by a 1° R change in water temperature.

The water-pump turbine valves can be replaced by fixed orifices sized for 100-percent design-point operation. Further simplification in control is possible above 47 percent power by keeping the bleed-pump turbine valves at their 100 percent settings. Below 47 percent power, the bleed-pump turbine valves must be controlled to delay the onset of pump stall.

The bleed-gas flow rate required no control in the range of this study. This system revealed a self-regulating tendency in which percent bleed rose as power and total hydrogen flow were decreased. In a modified system that bypassed some of the hydrogen around the heat exchanger, the operating envelope enlarged considerably and feasible steady-state operation was possible down to 13 percent power. Transient operation below this level may permit startup.

E-3439

INTRODUCTION

Extensive theoretical studies such as reference 1 have indicated the advantages of nuclear-powered vehicles in interplanetary missions. References 1 and 2 conclude that the weight required in orbit about Earth for manned Mars missions can be at least halved if nuclear propulsion is used instead of chemical propulsion.

Recent successful experimental reactor tests in the Nuclear Engine for Rocket Vehicle Application (NERVA) program (ref. 2) have increased the technical feasibility of nuclear propulsion in space. The NERVA reactor is a homogeneous, graphite-moderated reactor. Of the many problems surmounted in the NERVA program, some of the more troublesome were maintaining structural integrity of the core and combating the corrosive effects of chemical interaction of the hydrogen propellant with the graphite moderator (ref. 2).

In further support of the nuclear rocket effort, NASA has undertaken a thorough investigation of the heterogeneous class of reactor. The particular design receiving much attention is a thermal reactor having fuel elements of uranium mixed with tungsten enriched with tungsten-184 and using circulating water as the moderator. A feature of this concept is the negative temperature reactivities of the fuel and water moderator. This self-regulating characteristic not only acts as a built-in safety factor, but should aid in reactor-power control in response to any prescribed demand. Reference 3 points out other features, among which are low weight; high-temperature thermal-resistant characteristics and low neutron-absorption of the tungsten-184; and relief of the moderator structural problems by using a fluid moderator. The corrosion problem of interaction between propellant and moderator becomes nonexistent. Meanwhile, the integrity of the fuel-element design under extremes of temperature, radiation, and aerodynamic loading was investigated experimentally (ref. 4).

Aside from such reactor technical problems, the questions of stability, control, and operating feasibility of the integrated nuclear-engine system remained to be answered. For this purpose, NASA has made a complete system design with the tungsten water-moderated reactor as a power source in a combination bleed and topping cycle. In addition to the reactor, the system includes a water-hydrogen heat exchanger; a bleed system; bleed-driven water, hydrogen, and poison turbopumps; a topping turbopump; a regeneratively cooled thrust nozzle; a radiation shield; circulating poison; and associated valves and piping.

A preliminary version of the system design was used in the evolution of the program to improve the design and performance of the system. The system studied in the present investigation differs from a later version only by the absence of a cold-hydrogen gas passage around the heat exchanger.

As part of this program, the preliminary reference system was simulated on analog

computers so that the operation and control characteristics and interactions among the system parameters could be studied. This report presents the techniques used in the simulation and evaluates the accuracy of the results. A comparison of the computer results with detailed digital and hand calculations made individually of the heat exchanger, core, and turbopumps was employed in the validation.

The simulation was used in the present investigation to map system performance over a wide range of steady-state operation. By interpreting the steady-state maps obtained, the present report draws conclusions concerning the following aspects of system operation and control:

(1) Location and range of the feasible operating region

(2) Conditions restricting the operating range

(3) Search for suitable control parameters

(4) Merits and sensitivity of possible control parameters

(5) Simplifications in control by fixing system variables where possible

(6) Interactions among system parameters

(7) Suggested design modifications for improvement in system performance

The present analysis is one-dimensional, using a nonlinear analog computer simulation scaled primarily for use in the reactor power and flow range above 20 percent. Steady-state mapping was conducted by using hydrogen mass-flow rate and chamber temperature as independent variables. These parameters were varied over a range from 20 to 120 percent and from 67 to 135 percent of design, respectively. The wide range of variables gave assurance of encountering all constraints and even successive limits. The present study does not include startup, shutdown, malfunction, or transient operation.

DESCRIPTION OF SYSTEM

A brief description of the preliminary system follows. A schematic diagram of the flow system is given in figure 1 to aid in visualizing the hydrogen and water flow paths and the functions of the various components.

The heart of the system is the reactor core, which is a cylindrical aluminum tank containing a number of axially mounted aluminum tubes surrounded by water. Inside the tubes are fuel elements consisting of several concentric rings of fueled metallic cylinders mounted within a tungsten support tube. Hydrogen gas is heated as it flows through the annular passages between the rings. An aluminum pressure tube contains the concentric fuel-element assembly, and an annular region of stagnant hydrogen is provided between the tungsten support tube and the inner surface of the pressure tube. The stagnant hydrogen functions as an insulator between the high-temperature hydrogen and the moderator water. Another aluminum tube is mounted outside the pressure tube to act as a flow

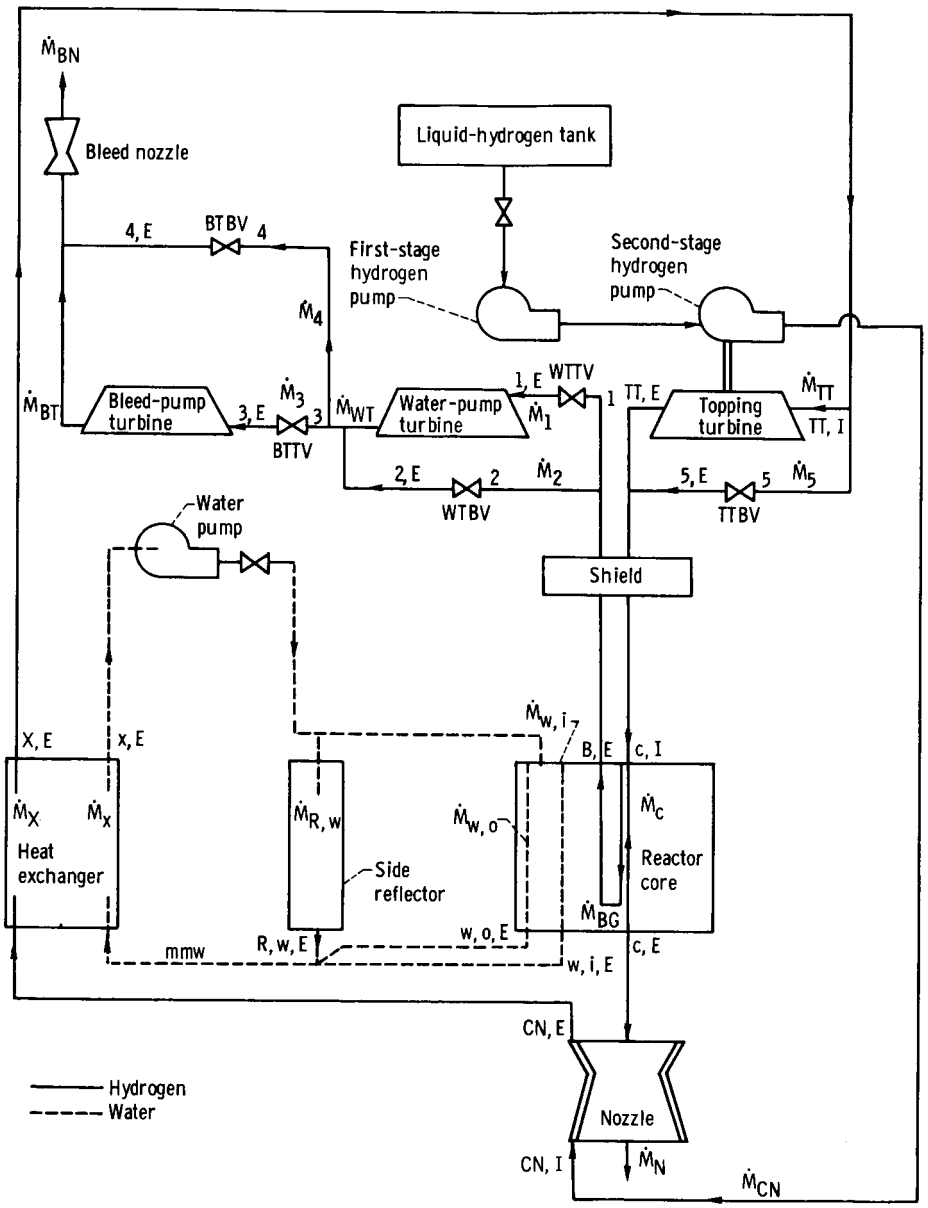

Figure 1. - Schematic flow diagram of tungsten water-moderated reactor preliminary reference system.

divider for the water. The moderator water is thus divided into a high-velocity region between the pressure tube and the flow divider, to enhance heat transfer, and a low-velocity region outside the flow divider. Several of the fuel assemblies are allocated for heating hydrogen for use in driving the bleed turbines. These fuel assemblies and the turbines along with the associated valves are referred to as the bleed system.

Hydrogen Flow Path

Liquid hydrogen from the tank is fed to the first- and second-stage hydrogen pumps in series (see fig. 1). They are referred to herein as bleed pump and topping pump, respectively. High-pressure hydrogen passes through nozzle cooling tubes for regenerative cooling and on to the heat exchanger. This is a shell-and-tube parallel-flow exchanger mounted just inside the reactor pressure vessel. Cold hydrogen flows through the tubes to cool the water flowing axially through the shell. The hydrogen is collected in a plenum at the heat-exchanger exit and ducted to the topping turbine, which drives the second-stage hydrogen pump. From the topping turbine the hydrogen reenters the pressure vessel, passes through a radiation shield, and into a plenum for distribution to the fuel elements. While flowing through the annular spaces between the fuel rings, the hydrogen gas is heated to an elevated temperature for discharge through the nozzle to produce thrust.

Water Flow Loop

The primary role of the circulating water is to function as the moderator in the reactor core, where it thermalizes the neutrons produced by fission. In addition, it cools the pressure tube, flow divider, and reflector, and delivers the heat absorbed in these components to the cold hydrogen in the heat exchanger.

The water loop is indicated by the dotted lines in figure 1. Water from the bleed-driven water pump enters an annular manifold inside the reactor pressure vessel where it is directed to the following three parallel paths: (1) high-velocity regions between the pressure tubes and the flow dividers, (2) low-velocity regions outside the flow-divider tubes, and (3) axial passages in the side reflector. The three water streams are collected and mixed in a plenum at the core exit. The direction of water flow is then reversed as the water enters the heat exchanger and flows axially through the shell side. Finally, it is returned to the water pump. The water system pressure is designed to match the core-gas exit pressure to minimize the loads on the outlet tube sheet.

Bleed Turbines

Bleed gas, heated to a suitable temperature level in the core, furnishes the energy to drive the two bleed turbines, which are in series. As shown in figure 1, the water-pump turbine is positioned upstream of the hydrogen bleed-pump turbine, which exhausts to the bleed nozzle. The order of the two bleed turbines in the series arrangement was dictated by a low limit of practical turbine blade height; that is, if the bleed-pump turbine were situated first in the series arrangement, its high rotational-speed requirement in combination with the high bleed-gas pressure would demand blade heights too short to be practical. The lower speed requirement of the water-pump turbine, however, permits it to be placed first without needing abnormally short blades.

During development of the turbine simulation in the present model, a preliminary study was made comparing parallel and series turbine arrangements. Strong interactions between the turbines were observed in response to valve changes in the series configuration. A vast improvement in turbine control became available by using a parallel arrangement, but this arrangement required the bleed-nozzle weight to be doubled and the bleed-flow requirements to be increased over 38 percent.

Controls

For control, the following six manipulated variables were provided in the system design to permit maximum flexibility in operation:

(1) Poison reactivity
(2) Water-pump-turbine throttle valve (WTTV)
(3) Water-pump-turbine bypass valve (WTBV)
(4) Bleed-pump-turbine throttle valve (BTTV)
(5) Bleed-pump-turbine bypass valve (BTBV)
(6) Topping-turbine bypass valve (TTBV)

SYSTEM MODEL

The present study used a nonlinear model of the preliminary reference system in which the following components were simulated on analog computers:

(1) Heat exchanger
(2) Core
(3) Reflector
(4) Bleed system

(5) Nozzle

(6) Turbopumps

(7) Valves

(8) Reactor kinetics

Three E.A.I. 231-R analog computers were used in the simulation using the following equipment: 287 amplifiers (including 53 integrators), 85 multipliers, 27 fixed and variable diode function generators, and 330 potentiometers.

The analysis, including the symbols, assumptions, basic equations, and application, is presented in appendixes A to D, respectively.

TABLE I. - NUMBER OF SECTIONS USED

IN MODEL COMPONENTS

Component	Equation		
	Energy	Momentum	Energy
	Number of sections		
	Axial		Radial
Core fuel assembly	3	---	1
Core gas	3	1	1
Core water	1	---	1
Reflector material	1	---	1
Reflector water	1	---	1
Bleed fuel assembly	1	---	1
Bleed gas	1	1	1
Heat-exchanger material	3	---	2
Heat-exchanger gas	3	1	1
Heat-exchanger water	3	---	1
Nozzle coolant	1	1	1

A summary of the number of sections used in the component simulations, where applicable, is presented in table I. As used herein, a section is defined as an imaginary subdivision in the representation of a component for use in applying finite-difference approximations to differential equations. Sections may be formed in the axial or radial directions, or both.

The simulation was scaled for the power and flow range above 20 percent. Startup and shutdown operations, which are not included in this study, would require rescaling throughout the system.

Heat Exchanger

The heat exchanger was represented in the simulation by a single tube, containing cold hydrogen gas flow, on the outside of which hot moderator water flowed. Both fluids flow in the same direction in the heat exchanger.

Gas. - Preliminary transient analog runs indicated that at least three axial sections were required for the heat-exchanger gas energy equation and one for the momentum equation. Dynamic traces of one- and two-section energy-equation models differed noticeably from those obtained by using three sections. Use of two or three sections to simulate the momentum equation, however, yielded no improvement over the use of one section. The length of each of the three sections for the energy equation is one-third of the heat-exchanger length.

Tubes. - Three axial sections were also used in the heat-exchanger material analysis to correspond with the three gas sections. Because of the high temperature gradient across the tube material (from hot water to cold hydrogen), it was found that one radial section was inadequate. Accordingly, two radial sections were used and the center temperature in each was calculated from the energy equation. With the assumption of a linear variation between the two radial-section center temperatures, the tube-surface temperatures were evaluated by extrapolation.

Water. - Three axial sections were used to simulate the heat-exchanger water energy equation. They correspond to the three axial sections used in the gas and tube material.

Core

Fuel assembly. - The concentric fuel rings were simulated by a single tube with a hydraulic diameter equivalent to that of the concentric assembly. On the basis of preliminary transient analog runs, the use of three axial sections was indicated for the reasons cited in the heat-exchanger discussion. The lengths of the first two sections are each one-fourth of the total length, whereas the third section is one-half the total. This selection of axial-section length was based on the axial reactor power distribution. One radial section was used.

Gas. - Three axial sections, corresponding to those used in the fuel assembly simulation, were used for the core-gas energy representation. Preliminary transient analog runs revealed that one axial section was adequate to simulate the momentum equation.

Water. - The water moderator flows through the core in units of two parallel passages separated by tubular flow dividers of aluminum. The array of pressure-tube - flow-divider units, with associated parallel water streams, that enclose the individual

fuel elements was represented by a single unit. Transient exploratory studies on the analog computer indicated a preference in using a one-axial-section, two-passage model instead of a three-axial-section, one-passage model. The flow split is assumed to be constant at the 100-percent design value.

Pressure tube and flow divider. - The pressure tube and flow divider were each simulated by one axial and one radial section. Therefore, the temperature of each was assumed constant throughout the material.

Reflector

The side reflector was represented by a single equivalent beryllium cylinder. A single passage through the reflector material represented the many passages in the actual design.

Material. - One axial section was used in the reflector-material simulation.

Water. - A one-axial-section model was also used for the reflector water. The water mass-flow rate through the reflector was assumed to be proportional to the total circulating-water flow rate.

Bleed System

The bleed gas makes two passes through the core. In the first pass, both the pressure drop and heat absorbed by the bleed gas are relatively small. Therefore, only the second pass was simulated. The shield was not simulated in detail. The heat given up by the bleed gas to the shield, water, and cold hydrogen at the inlet-hydrogen plenum was assumed proportional to the bleed-gas exit temperature.

Fuel assembly. - A single tube was used to represent the fuel elements allocated for heating the bleed gas. One axial and one radial section were used.

Gas. - One axial section was used for both the energy and momentum equations of the gas in the bleed system.

Nozzles

Coolant. - Highly accurate nozzle-coolant calculations require many more than the one, two, or three sections feasible in analog work. Therefore, it was concluded that one section would be used to represent both the nozzle-coolant energy and momentum equations. During development of the nozzle model, exploratory analog calculations revealed that a one-section model yielded a momentum-pressure drop that was more

representative than either two- or three-section models. The comparison was made with results obtained from digital calculations in which 49 sections were used.

Turbopumps

The turbine and pump characteristics were represented by appropriate functions set on variable diode function generators. Details are presented in appendix D.

Valves

The four bleed valves and the topping-turbine bypass valve were simulated by equations presented in appendix D. Provision was made for both choked and nonchoked valve performance as applicable.

Reactor Kinetics

The neutron kinetics was represented by a one-energy group, space-independent model with six groups of delayed neutrons. Negative reactivity feedbacks were provided in response to the average temperatures of the fuel and core water. The positive contribution to reactivity of the core-gas density is negligible in the range of this investigation.

VALIDATION

After each computer was implemented with its part of the simulation, a static check was made to verify the scaling in the equations and computer patching. System conditions at the 100-percent design point were used in making the static checks.

In addition to the 100-percent design point, conditions at two other arbitrarily selected reference points were determined for use in further checking of the model. These were at 60 and 36.6 percent of design mass-flow rate and at design chamber temperature. Conditions at these three reference points (100, 60, and 36.6 percent) were obtained from independent detailed digital and hand calculations made individually of the heat-exchanger, core, and turbopumps. As an aid in making the analog computations, controls were placed on poison reactivity and the topping-turbine bypass valve to set chamber temperature and core-gas mass-flow rate, respectively. Details of these controls will be presented subsequently.

TABLE II. - DEVIATION OF ANALOG RESULTS COMPARED WITH DIGITAL- AND HAND-CALCULATED RESULTS AT THREE REFERENCE POINTS

Variables	Percent of design value		
	100	60	36.6
	Deviation, percent		
Reactor power	-0.93	0	0
Hydrogen mass-flow rate through heat-exchanger, $\dot{M}_X$	3	0	0
Bleed-pump exit pressure, $P_{BP,E}$	0.74	0.84	0
Coolant-nozzle inlet pressure, $P_{CN,I}$	1.54	1.6	-14
Coolant-nozzle exit pressure, $P_{CN,E}$	0.55	-2.5	-2.6
Hydrogen pressure at heat exchanger exit, $P_{X,E}$	0.84	-1.1	-0.6
Hydrogen temperature at heat exchanger exit, $T_{X,E}$	-0.33	0	-3.4
Topping-turbine rotational speed, N_{TT}	-0.11	0	-11.8
Topping-turbine mass-flow rate, $\dot{M}_{TT}$	3.1	0	-14.5
Mass-flow rate through topping-turbine bypass valve, $\dot{M}_5$	-11.9	-0.87	15.1
Hydrogen pressure at core inlet, $P_{c,I}$	0.57	-0.37	0.76
Hydrogen temperature at core inlet, $T_{c,I}$	-0.31	0	-3.3
Hydrogen mass-flow rate in core, $\dot{M}_c$	0	0	0
Hydrogen pressure at core exit, $P_{c,E}$	-0.5	-0.69	-0.22
Hydrogen temperature at core exit, $T_{c,E}$	0	-0.04	0
Bleed-gas mass-flow rate, $\dot{M}_{BG}$	0	0	-0.45
Pressure at water-pump turbine throttle valve inlet, P_1	-1.2	-0.82	-3.4
Temperature at water-pump turbine throttle valve inlet, T_1	-1.8	-0.43	-0.48
Mass-flow rate through water-pump turbine throttle valve, $\dot{M}_1$	.16	-0.66	-1.7
Mass-flow rate through water-pump turbine bypass valve, $\dot{M}_2$	-0.63	1.5	1.2
Water-pump turbine rotational speed, N_{WT}	0	0	0
Pressure at water-pump turbine bypass valve exit, $P_{2,E}$	-2.0	-1.1	-3.7
Temperature at water-pump turbine bypass valve exit, $T_{2,E}$	-1.7	-0.44	-0.49
Mass-flow rate through bleed-pump turbine throttle valve, $\dot{M}_3$	-0.31	-0.23	-1.6
Mass-flow rate through bleed-pump turbine bypass valve, $\dot{M}_4$	1.3	-0.18	1.9
Bleed-pump turbine rotational speed, N_{BT}	-0.18	0	0
Pressure at bleed-pump turbine bypass valve exit, $P_{4,E}$	-3.4	-5.6	-6.7
Temperature at bleed-pump turbine bypass valve exit, $T_{4,E}$	-1.82	-0.47	-0.46
Water mass-flow rate through heat exchanger, $\dot{M}_x$	0	0	-0.44
Pressure at water-pump exit, $P_{WP,E}$	0	0	0
Mixed mean water temperature, T_{mmw}	0.06	1.8	-0.23
Water temperature at heat-exchanger exit, $T_{x,E}$	-0.28	2.0	-0.05

In order to check a reference point, the water-pump turbine throttle and bypass valves were first set at the reference positions. Then, minor adjustments (from the reference settings) were made to the bleed-pump-turbine throttle and bypass valves until simultaneous reference values were obtained for the core-gas exit temperature, core-gas mass-flow rate, bleed-gas mass-flow rate, bleed-turbine mass-flow rate, and both bleed-turbine rotational speeds. Friction terms in the bleed system and water loop were trimmed slightly to attain the reference values. Steady-state data were recorded of all calculated parameters for comparison with the digital reference values.

In table II (p. 11) are presented the percent deviations from the results of digital calculations of some of the more significant system variables at each of the three reference points. It is immediately apparent that the only large deviations are in the topping turbopump, primarily at the 36.6-percent point. In the initial setting of this point, it was observed that the turbopump variables agreed closely but the value of core-inlet pressure deviated slightly from the check point. Therefore, the friction in the lines joining the topping turbine with both the heat exchanger and core was adjusted to approach closely the reference value of core-inlet pressure. Friction settings that distributed the errors in these components evenly resulted in deviations of the order of 5 percent in each; however, it was considered more important to the performance of the rest of the system to achieve reference conditions in the core.

It is shown in table II that most of the other deviations throughout the system are of the order of 1 percent, with only two greater than 5 percent. A 5-percent error is considered acceptable for a nonlinear analog study of the magnitude undertaken herein.

MAPPING PROCEDURE

Three complete sets of steady-state maps were obtained. A set was made with the four bleed valves (water-pump-turbine throttle and bypass valves, and bleed-pump-turbine throttle and bypass valves) positioned at the 100-, 60-, and 36.6-percent reference points. These settings provided a topping-to-bleed-pump work split of 2 to 1 at each of the three reference points. The reason for maintaining fixed bleed-valves settings in the mapping survey was to determine if system control could be simplified by eliminating the need for these four manipulated variables.

In order to expedite the data-taking process, proportional-plus-integral controls were placed on the poison reactivity and topping-turbine bypass valve, as was done in the validation study. The controls automatically regulated these two components to yield values of core-gas exit temperature $T_{c,E}$ (chamber temperature) and core-gas mass-flow rate $\dot{M}_c$ in response to preselected demand signals. The controls were simulated by the following transfer functions:

For $T_{c,E}$,

$$\frac{\delta k'_p}{\epsilon_T} = -\left(K_{1,T} + \frac{K_{2,T}}{s}\right) \tag{1}$$

for $\dot{M}_c$,

$$\frac{c_{v,5}}{\epsilon_{\dot{M}}} = K_{1,\dot{M}} + \frac{K_{2,\dot{M}}}{s} \tag{2}$$

The error terms are the differences between demand and output signals; that is,

$$\epsilon_T = (T_{demand} - T)_{c,E} \tag{3}$$

and

$$\epsilon_{\dot{M}} = (\dot{M}_{demand} - \dot{M})_c \tag{4}$$

With the mass-flow control set to maintain the topping-turbine bypass valve at a fixed position, a survey was made in the temperature range between 3000° and 6000° R by adjusting the demand signal of the chamber-temperature control to yield data at several selected values of $T_{c,E}$. After a traverse at constant hydrogen mass-flow rate, the topping-turbine bypass valve was repositioned by setting a different demand in the mass-flow control, and chamber temperature was again varied through its control. This procedure was repeated while the mass-flow rate was maintained constant at values of 20, 30, 36.6, 40, 50, 60, 70, 80, 90, 100, 110, and 120 percent of the design value. The ranges of $T_{c,E}$ and $\dot{M}_c$ were wide enough to provide data well beyond the design constraints. In fact, as $T_{c,E}$ was raised at a fixed mass-flow rate setting, four successive constraints were exceeded. Thus, if one of a series of constraints should be relaxed in the future, the margins from the next successive limitation would be available.

The constraints applied to the mapping investigation of the system are as follows:

Fuel temperature rise, $^{\circ}$R	83
Nozzle-wall temperature rise, $^{\circ}$R	65
Water-pump turbine-inlet temperature rise, $^{\circ}$R	100
Pressure-tube temperature rise, $^{\circ}$R	20
Heat-exchanger minimum water-side wall temperature, $^{\circ}$R	492
Bleed-pump stall, $\left[(\dot{M}/N)/(\dot{M}/N)_{des}\right]_{BP,min}$	0.723
Turbine rotational speed rise, percent	10

RESULTS AND DISCUSSION

The first important result of this study is that the system could be maintained at steady-state conditions with no external feedback controls. It was not known prior to operation of the simulation on the analog whether or not the engine system could be maintained at steady-state conditions without closed-loop controls.

The data obtained are plotted in figures 2 to 4 for bleed-valves settings corresponding to the 100-, 60-, and 36.6-percent reference points, respectively. All these figures are drawn over a background map of chamber pressure plotted against chamber temperature with constant core-gas mass-flow rates. Chamber temperature is used as a coordinate because it is a primary factor in rocket specific impulse. Core-gas mass-flow rate and chamber pressure are representative of thrust. The variation in chamber temperature on the maps is restricted to the range between 3000° and 6000° R to provide increased sensitivity.

The background maps are all the same, irrespective of bleed-valves settings. Parts (a) present the locations of the various engine constraints. Parts (b) to (g) show curves of constant values of some of the more significant engine variables. In addition, constraint boundaries pertaining to the appropriate bleed-valves settings are located in parts (b) to (g) of figures 2, 3, and 4. Four overlays are available on request for comparing the locations of the constraint boundaries obtained from one set of bleed-valves settings with those of the other two sets. A request card for the overlays is bound at the back of the report. Study of the equations in appendix D should prove helpful in understanding the behavior of the system and in following the trends brought out in the subsequent discussions.

Constraints

100-percent bleed-valves settings. - Figure 2(a) reveals that with the bleed valves set at the 100-percent positions a feasible operating region extends from about 52 to 120 percent of the design core-gas mass-flow rate with bleed-pump stall and speed limits forming the lower and upper boundaries. However, heat-exchanger freezing and the nozzle-wall temperature limit confine the allowable chamber temperature to a corridor between about 4000° and 4500° R. The margin of the design point from heat-exchanger freezing is greater than from the nozzle-wall temperature limit.

It is evident from figures 2(a), 3(a), and 4(a) that the main hindrance to low-flow operation is the onset of stall in the hydrogen bleed pump. This observation indicates that as the total system mass-flow rate is reduced at constant bleed-valves settings, the bleed pump assumes a greater fraction of the load.

Of primary significance in figure 2(a) is the intersection of the bleed-pump stall and

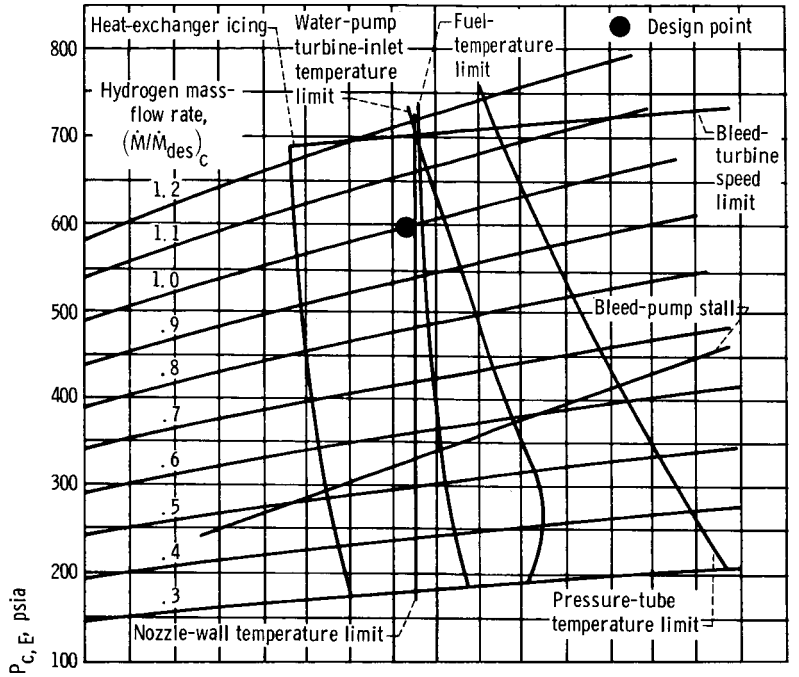

(a) Constraints.

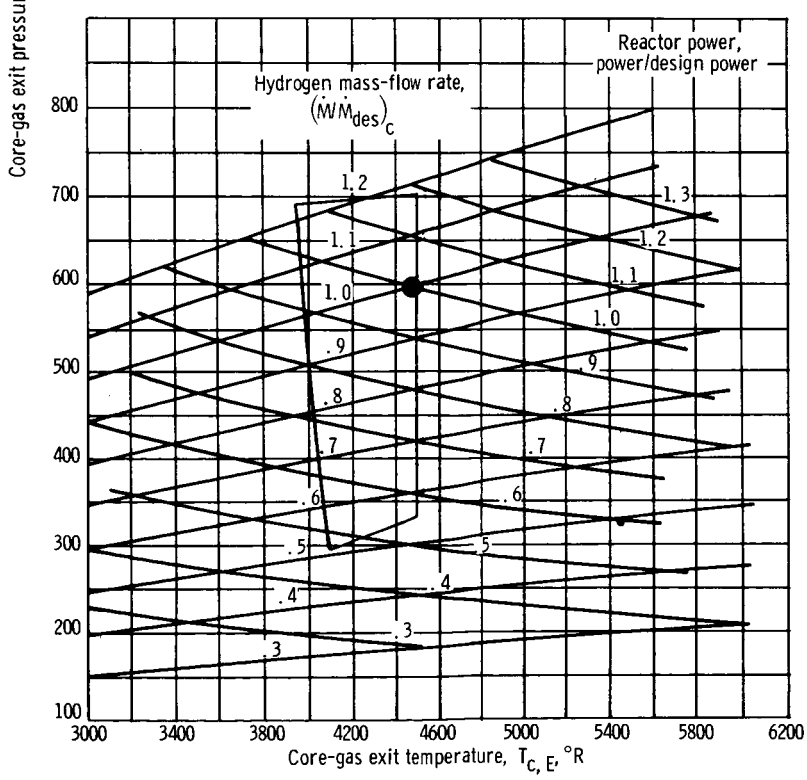

(b) Reactor power.

Figure 2. - Steady-state maps of tungsten water-moderated reactor preliminary reference system with 100-percent bleed-valves settings.

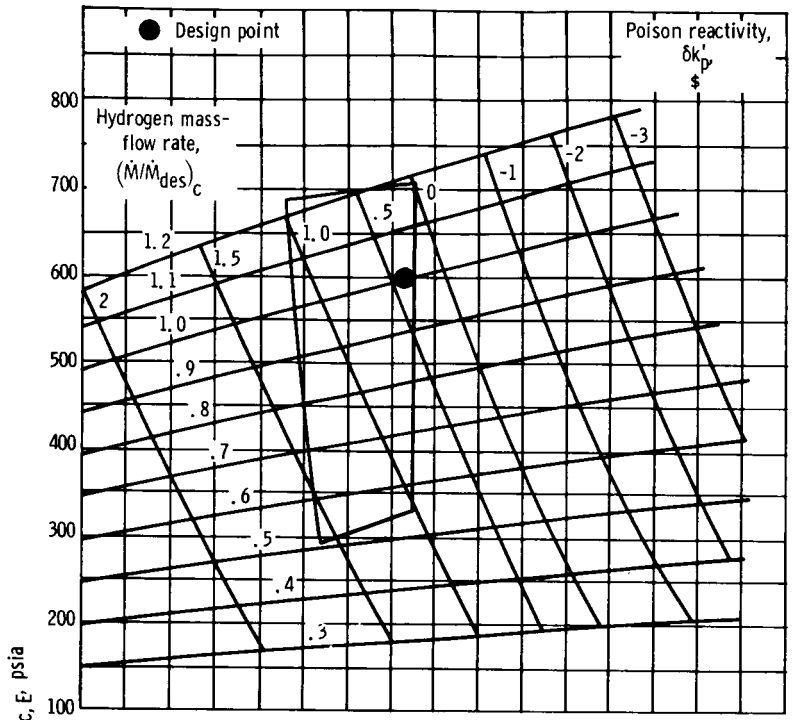

(c) Poison reactivity.

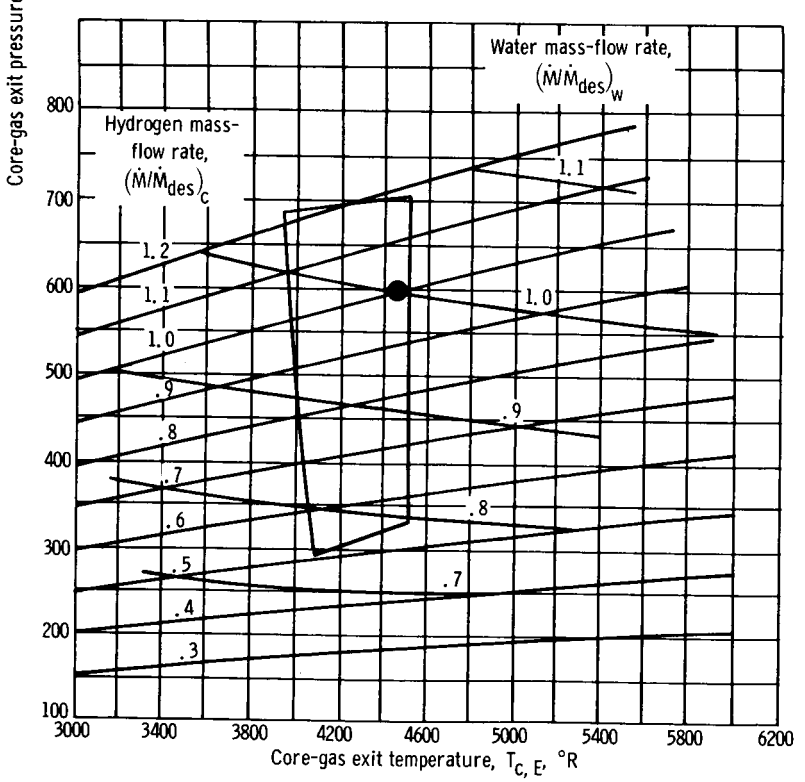

(d) Water mass-flow rate.

Figure 2. - Continued.

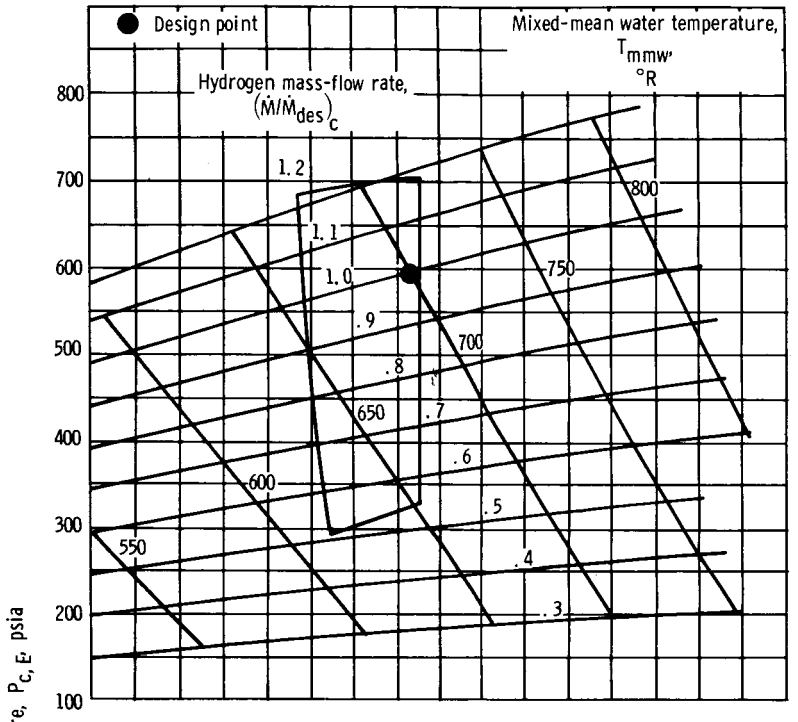

(e) Mixed-mean water temperature.

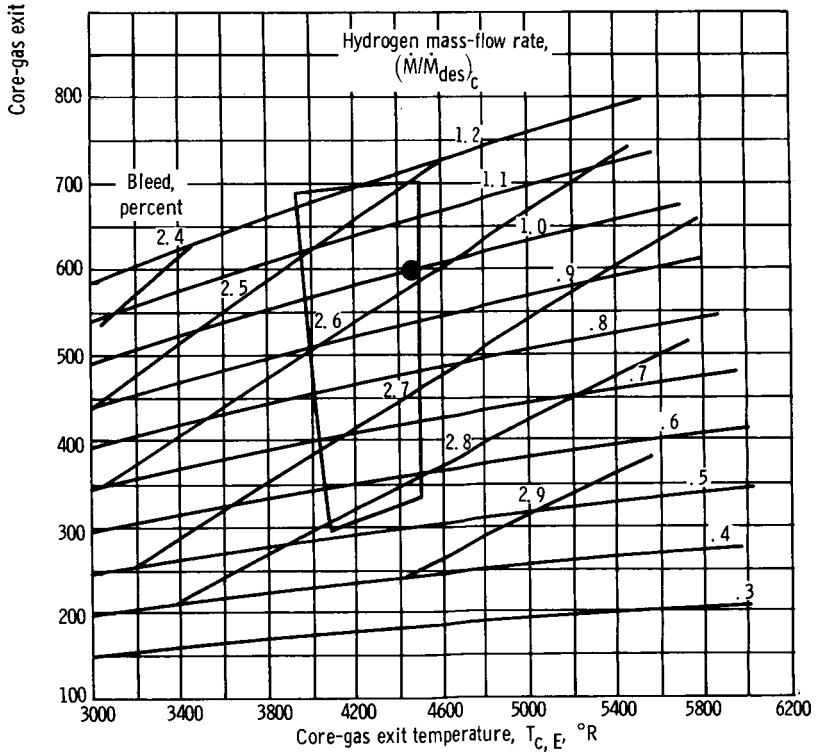

(f) Percent bleed.

Figure 2. - Continued.

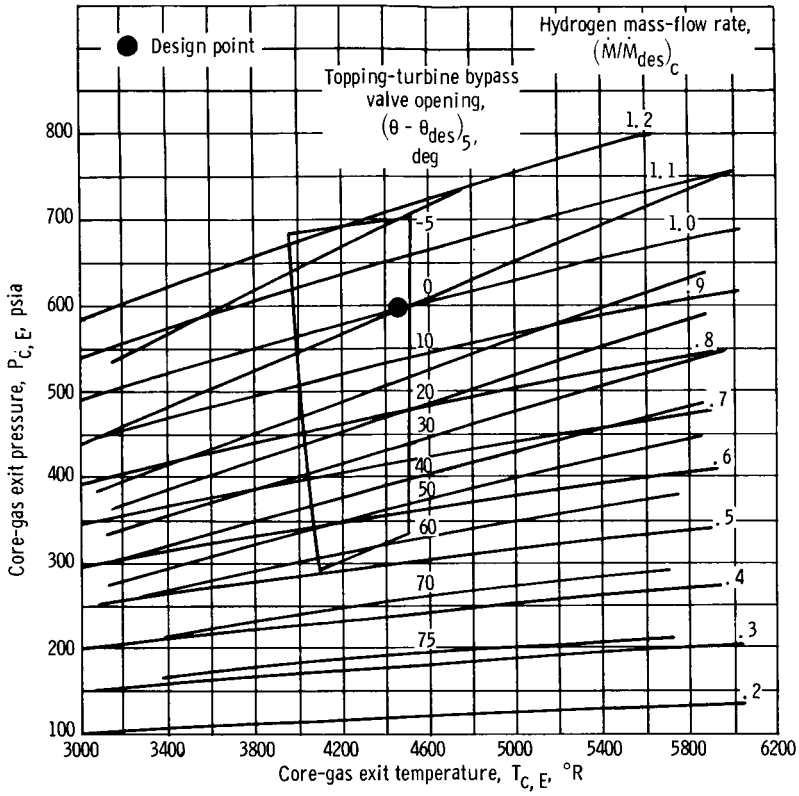

(g) Topping-turbine bypass valve setting.

Figure 2. - Concluded.

heat-exchanger freezing curves. This intersection, at about 52 percent of design core-gas mass-flow rate and 47 percent of design reactor power, establishes a lower limit to steady-state operation of the preliminary reference system with 100-percent bleed-valves settings. Thus, the attempt to simplify system control by fixing the four bleed valves at the 100-percent settings was not altogether successful. The simplification is feasible above approximately 47 percent of design power provided that the system is operated to maintain the chamber-temperature level within the 500° R range indicated in figure 2(a).

Figure 2(a) reveals that neither the water-pump turbine-inlet temperature nor the pressure-tube temperature is limiting when the bleed valves are set at their 100-percent positions. Bleed-pump turbine rotational speed sets an upper bound to the operating region, but at mass-flow rates considerably higher (120 percent) than the system 100-percent design point. The 110-percent bleed-pump rotational-speed constraint was specified to avoid exceeding the allowable stresses in the pump and turbine blades.

60-percent bleed-valves settings. - When a different set of bleed-valves positions is used, it is evident that the bleed system, water loop, and any parameters affected thereby will experience changes. Figure 3(a) presents the locations of the various constraints for the 60-percent bleed-valves settings. Comparison of figures 2(a) and 3(a) or placing

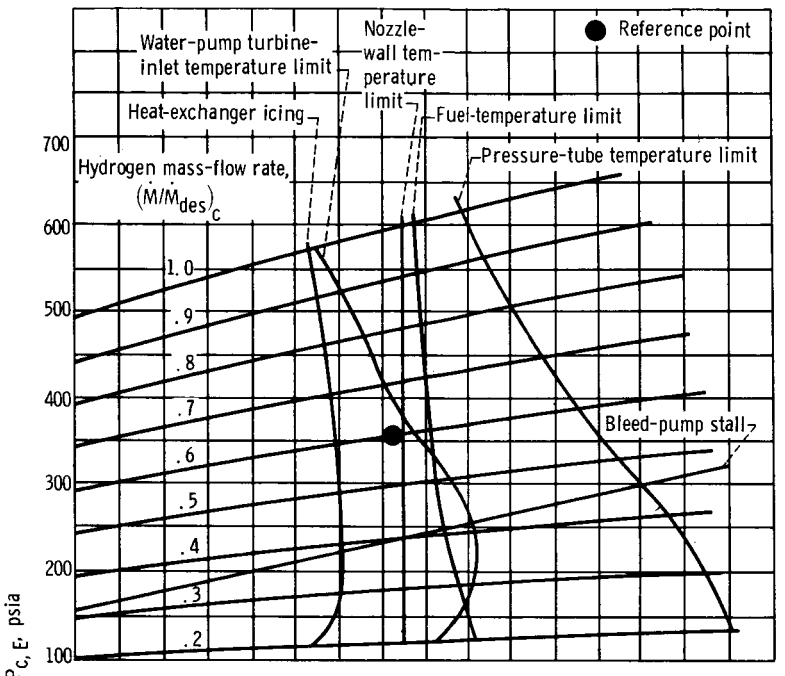

(a) Constraints.

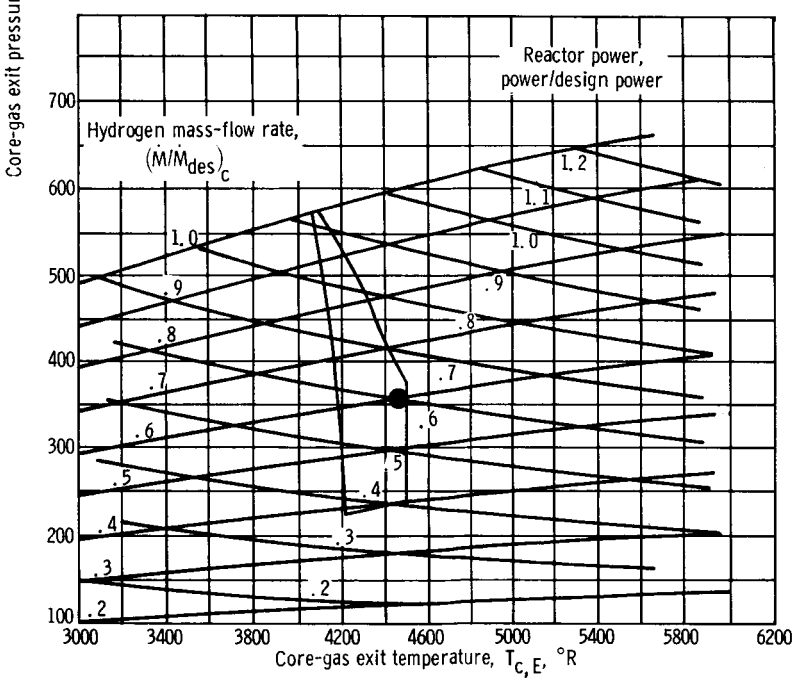

(b) Reactor power.

Figure 3. - Steady-state maps of tungsten water-moderated reactor preliminary reference system with 60-percent bleed-valves settings.

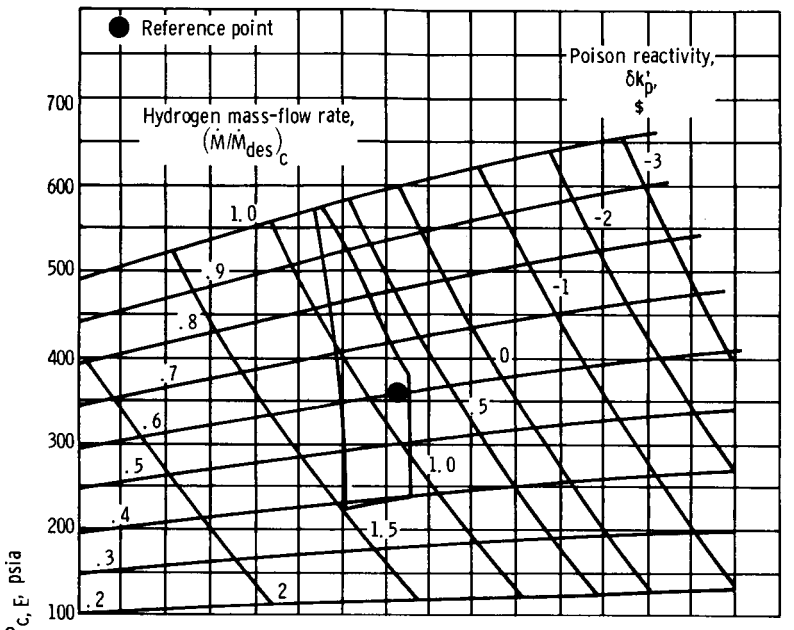

(c) Poison reactivity.

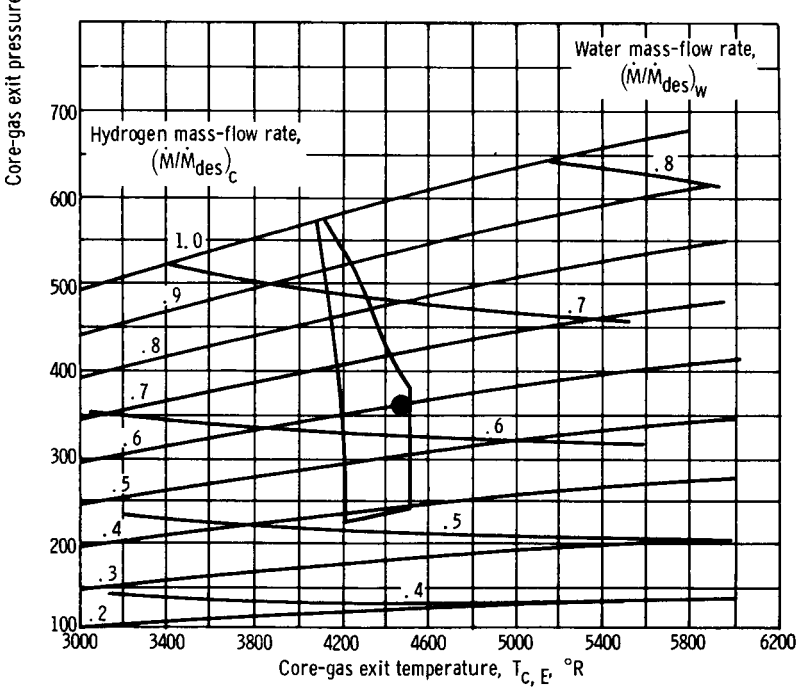

(d) Water mass-flow rate.

Figure 3. - Continued.

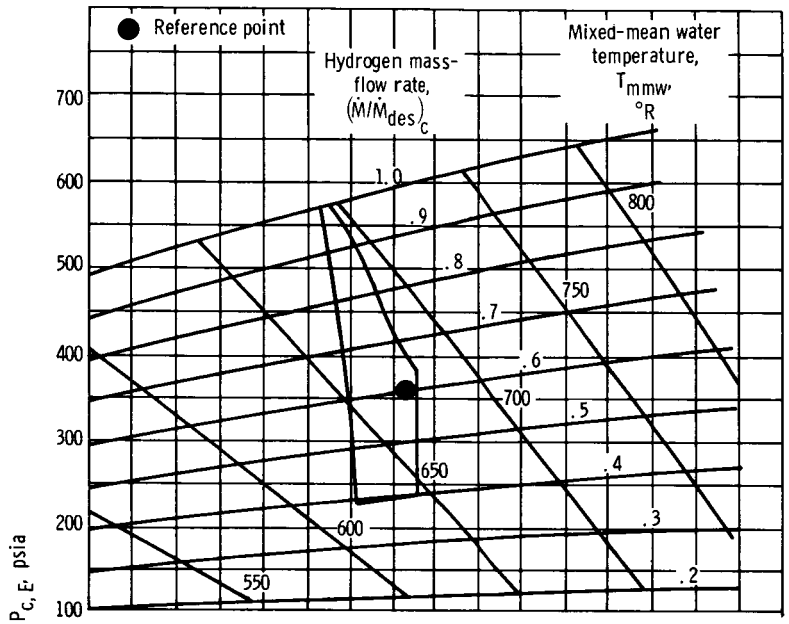

(e) Mixed-mean water temperature.

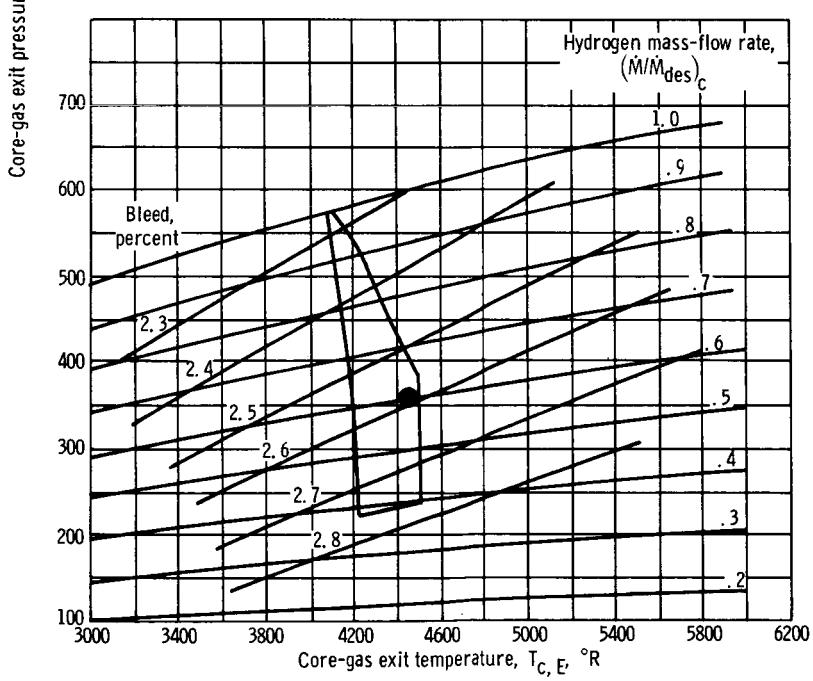

(f) Percent bleed.

Figure 3. - Continued.

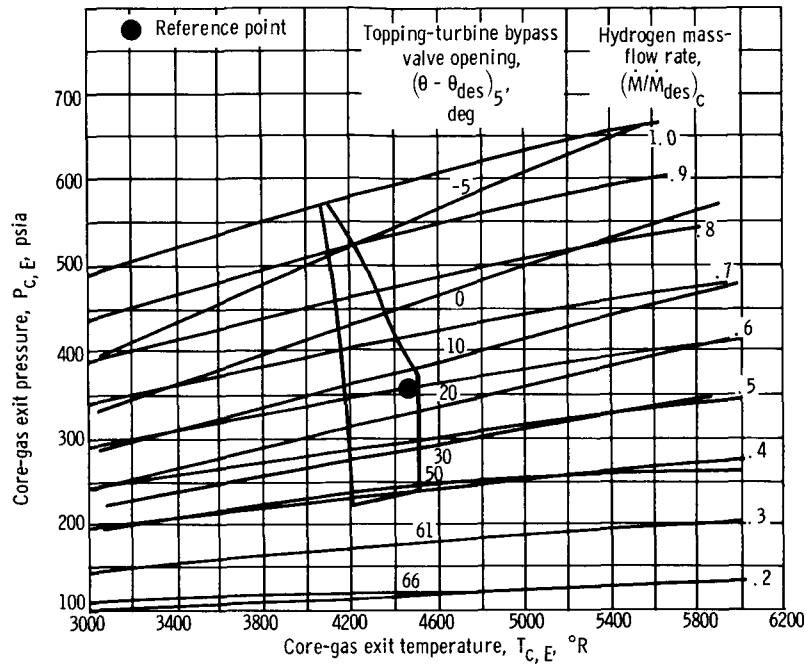

(g) Topping-turbine bypass valve setting.

Figure 3. - Concluded.

overlay 1 on figure 3(a) shows that changing the bleed-valves positions merely shifts the locations of the bleed-dependent constraints on the background map of chamber conditions. Only the nozzle-wall and fuel temperature limit curves are unaffected by the change in bleed-valves settings. Location of the nozzle-wall temperature limit curve is not altered because this temperature is assumed to be proportional to the chamber temperature (see appendix B and ref. 5). The fuel temperature is not influenced by the bleed system. For any given combination of core-gas exit pressure, temperature, and mass-flow rate, there is a corresponding value of fuel temperature. Any differences between the T_F curves of figures 2(a) and 3(a) are minor and result from slight changes in heat-transfer coefficients and gas properties.

The most noticeable feature of the comparison of figures 2(a) and 3(a) or of overlay 1 and figure 3(a) is the drastic reduction in the feasible operating region that results from adjusting the bleed valves to the 60-percent settings. The operating corridor is narrowed as the heat-exchanger icing curve is displaced to a position of higher chamber temperature, while the water-pump turbine-inlet, and pressure-tube temperature limits are located at lower chamber-temperature positions. Displacement of the pressure-tube temperature-limit curve can be seen by comparing figures 2(a) and 3(a) or by placing overlay 2 on figure 2(a).

On the other hand, closing down the bleed valves has the advantage of lowering the bleed-pump stall curve. At the 60-percent bleed-valves settings, the stall and heat-

exchanger freezing intersection occurs at about 39 percent of design flow and 37 percent of reactor power. As before, the bleed pump assumes a greater fraction of the load as the system mass-flow rate is lowered. When the bleed-pump-turbine throttle valve setting is reduced to the position corresponding to the 2-to-1 pump power split at the 60-percent point, however, the load fraction taken by the bleed pump for any given set of chamber conditions is lowered. Therefore, the onset of bleed-pump stall is postponed during reduction of system mass-flow rate so that the stall line is lowered to the location shown in figure 3(a).

The opposing effects of heat transfer to and from the water in the core and heat exchanger (to be discussed subsequently) differ from those occurring at the 100-percent bleed-valves settings; thus, the heat-exchanger freezing curve is displaced to a more restrictive location in figure 3(a).

At the reduced openings of the bleed valves, the bleed-flow rate is below that required for adequate cooling of the bleed fuel assemblies at many points in figure 3(a) above a chamber temperature of 4200° R. The resulting rise in bleed-gas temperature causes the allowable water-pump turbine-inlet temperature to be exceeded, as shown by the latter curve cutting through the operating region of figure 3(a). Design chamber-temperature operation is unobtainable above approximately 67 percent of flow and power.

Thus, the water-pump turbine-inlet temperature has replaced the nozzle-wall temperature as a primary constraint. An obvious way to avoid this restriction would be to open the water-pump-turbine and bleed-pump-turbine bypass valves to allow increased mass-flow rate through the bleed fuel elements. Doing so, however, would depart from the attempt to maintain constant bleed-valves settings. If, however, the limitation on T_1 could be relaxed to permit turbine operation at 2050° R, most of the region between the heat-exchanger freezing and nozzle-wall temperature limits (including the 100-percent design point) would become available. Opening the operating region in this way to simplify control by fixing the bleed valves at the 60-percent settings would require advanced turbine technology, such as the use of higher-temperature-resistant materials or turbine cooling.

Another interpretation of this observation is that in order for the bleed-pump turbine to develop the amount of work needed to achieve the 100-percent design point, its inlet temperature and therefore T_1 must rise to 2050° R owing to the decrease in bleed-gas mass-flow rate.

Closing down the bleed valves also decreases the water mass-flow rate at any point on the map in figure 3(a). Therefore, the pressure-tube temperature rises because of the reduction in the heat-transfer coefficient h_i caused by lowering the factor $\dot{M}_{w,i}^{0.8}$ in equation (D82). This explains the leftward displacement of the pressure-tube temperature constraint on the map.

36.6-percent bleed-valves settings. - Examination of figure 4(a) reveals that an even smaller operating region is available when the 36.6-percent bleed-valves settings are

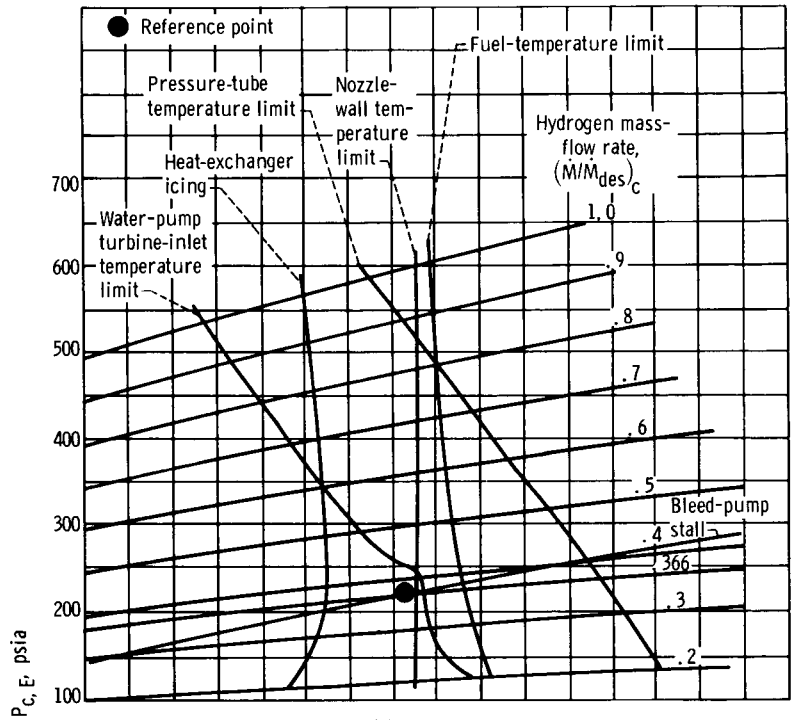

(a) Constraints.

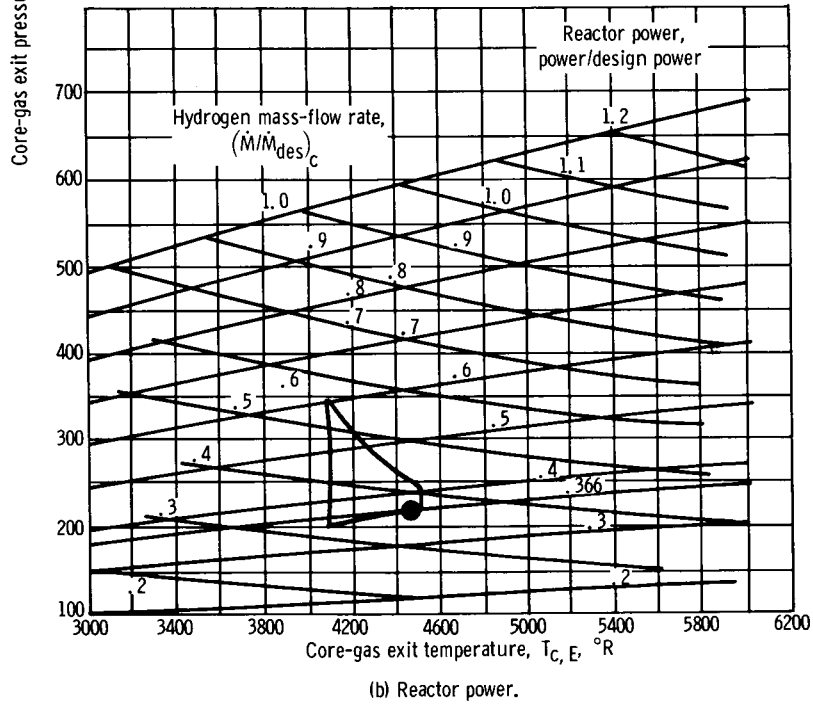

Core-gas exit pressure, $P_{c,E}$, psia

(b) Reactor power.

Figure 4. - Steady-state maps of tungsten water-moderated reactor preliminary reference system with 36.6-percent bleed-valves settings.

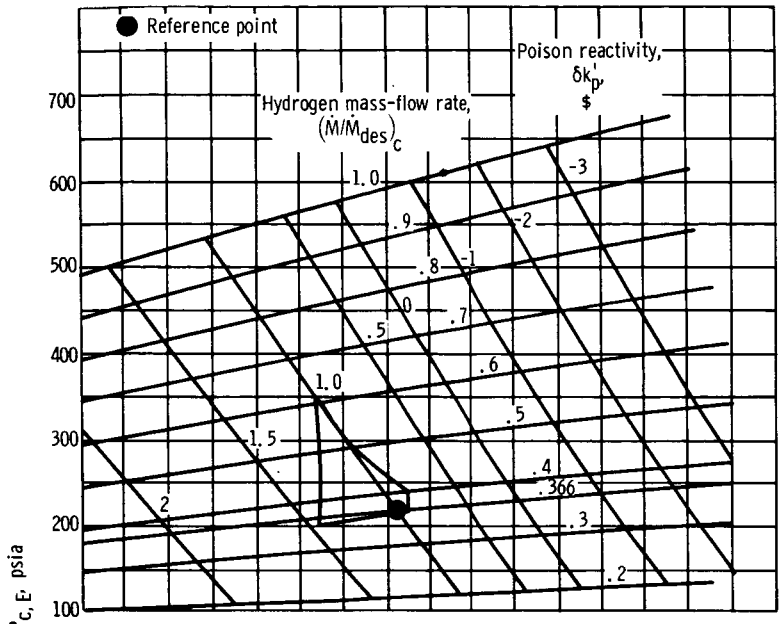

(c) Poison reactivity.

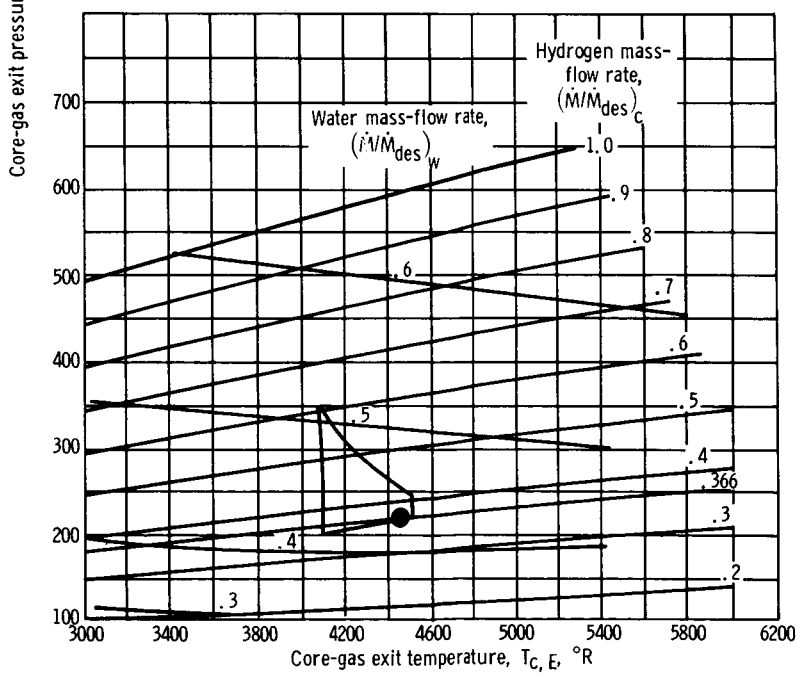

(d) Water mass-flow rate.

Figure 4. - Continued.

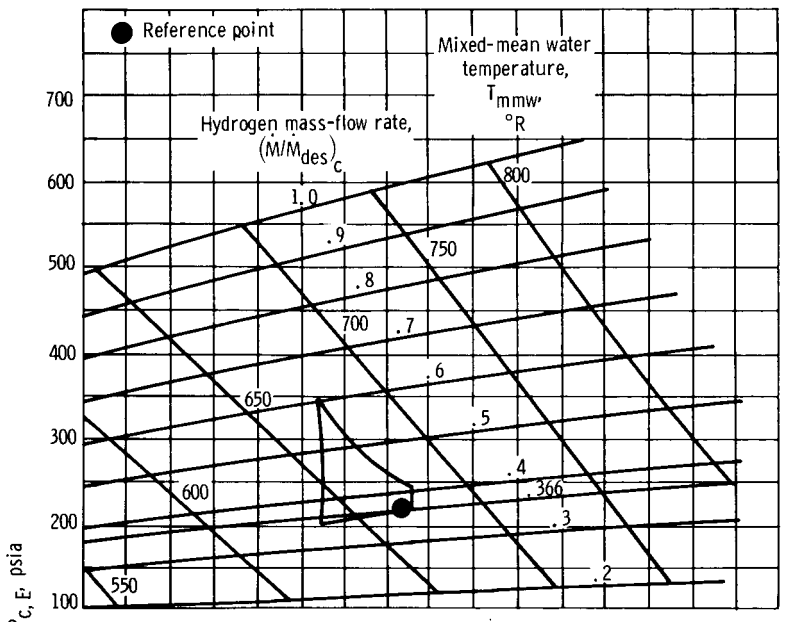

(e) Mixed-mean water temperature.

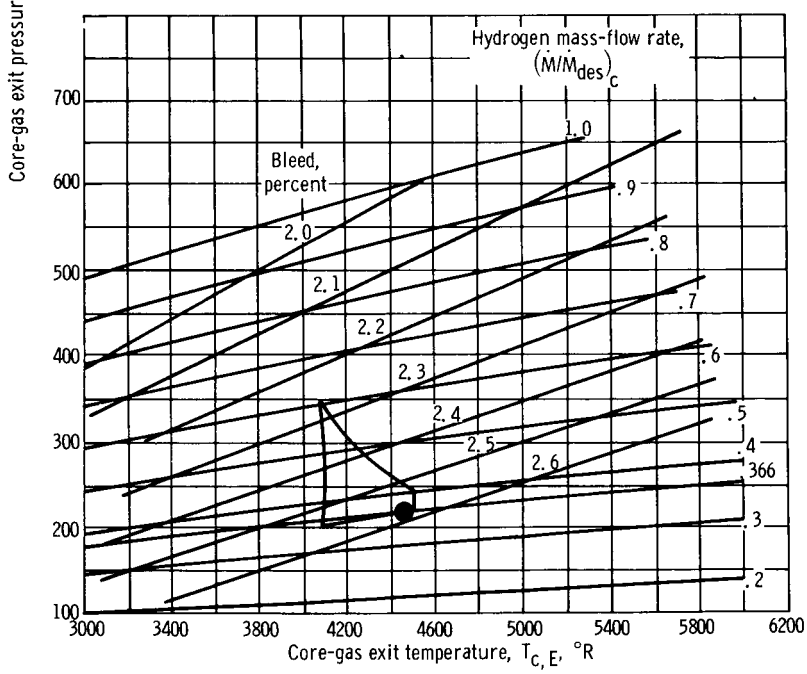

(f) Percent bleed.

Figure 4. - Continued.

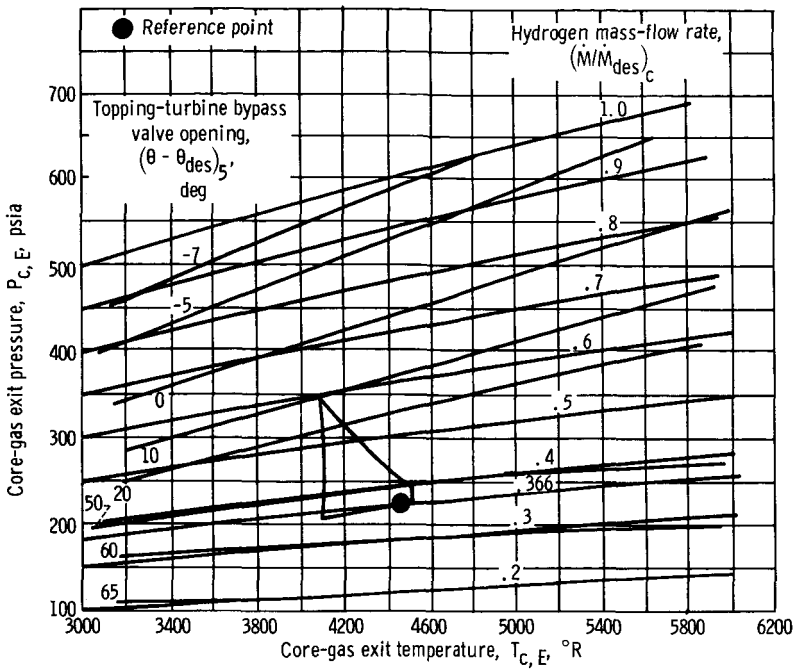

(g) Topping-turbine bypass valve setting.

Figure 4. - Concluded.

used. The water-pump turbine-inlet temperature constraint cuts deeply through the corridor bounded by heat-exchanger icing and the nozzle-wall temperature limit to eliminate most of this envelope. The pressure-tube temperature limit also passes through this region. Meanwhile, however, the bleed-pump-stall curve is lower, and the heat-exchanger icing limit is relocated approximately at its position for the 100-percent settings. The nozzle-wall and fuel temperature limit boundaries are unchanged.

With the 36.6-percent settings, the intersection of the bleed-pump stall and heat-exchanger icing limitations occurs at about 35 percent of design flow and 33 percent of power. In fact, the 36.6-percent reference point itself lies on the bleed-pump stall line. Design chamber-temperature operation is restricted to mass-flow rates in the range between 37 and 42 percent of design. The small operating region available with 36.6-percent bleed-valves settings indicates that it would not be fruitful to operate with bleed-valves settings of less than the 60-percent positions.

Comparison of figures 2(a) and 4(a) or placing overlay 1 on figure 4(a) shows that a larger operating region would be available with 36.6 percent settings than with 100-percent settings if the water-pump turbine-inlet temperature limit could be relaxed. The lowered stall curve at 36.6 percent accounts for this observation. It would be a distinct advantage in control if operation maneuvers throughout this region could be performed without requiring changes in the bleed-valves settings. To achieve the 100-percent design point, however, a temperature of 2300° R is required at the water-pump turbine

inlet. Even if this were possible, 100-percent design-point operation would be denied by the pressure-tube temperature constraint.

Composite Map

In order to present the overall feasible operating region, a composite map of figures 2(a), 3(a), and 4(a) was drawn. The resulting plot is shown in figure 5 as a plot of percent reactor power against hydrogen mass-flow rate. In the production of this figure, a continuous transition of constraint boundaries was assumed between figures 2(a) and 3(a) and between 3(a) and 4(a). Note that this plot is, in effect, merely a section of the bleed-pump head-flow performance map. Steady-state operation is confined to the enclosed region, which is bounded by the bleed-pump stall curve at the lower end and by one of its speed curves at the upper end. A temperature limit in the nozzle wall bounds the upper side, and heat-exchanger freezing, the lower.

The map in figure 5 summarizes the data presented in figures 2(a), 2(b), 3(a), and 4(a). Its main advantage lies in providing an overall perspective of the capabilities and shortcomings of the preliminary reference design. The previously mentioned freezing-stall intersection establishing the lower bound of feasible steady-state operation at 33 percent of design reactor power is prominent. From this observation, the steady-state results indicate that startup of the preliminary reference system may be a major problem. A conclusive determination of the startup capability of this system would require a detailed transient investigation in the low-power range.

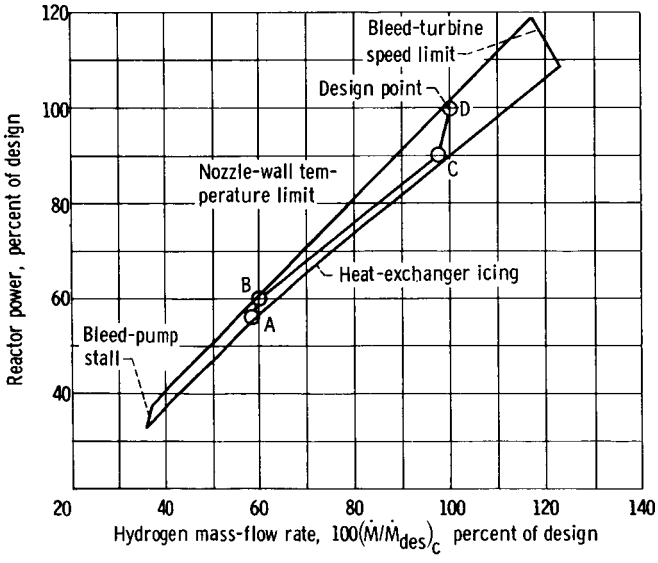

Figure 5. - Composite steady-state operating map of tungsten water-moderated reactor preliminary reference system.

The margin of the 100-percent design point from heat-exchanger icing is much greater than that from the nozzle-wall temperature limit. Design chamber-temperature is represented, although not shown, by a 45° line through the origin in figure 5. This 45° line lies just within the nozzle-wall temperature-limit boundary in figure 5. Thus, design specific impulse is potentially obtainable within the operating envelope above the 36.6-percent reference point. Although marginally obtainable in steady-state operation, design chamber temperature may be unobtainable from a practical standpoint where adequate margins are required.

The gradual narrowing of the operating corridor in figure 5 shows that in the preliminary reference system the heat-exchanger problem becomes more serious with decreasing system mass-flow rate.

Engine Parameters

Variations in some of the more important engine parameters are presented in figures 2(b) to (f), 3(b) to (f), and 4(b) to (f). In these figures, constant values of each parameter are plotted on the same background as that used in the discussion of constraints. Therefore, the superimposed constraint boundaries on the engine-parameter figures show the range of variation of the given parameter within the operating region. In the presentation that follows, most of the discussion is directed to figure 2 (100-percent bleed-valves settings) because it is typical of the values obtainable from figures 3 and 4.

Reactor power. - The plot of figure 2(b) presents curves of constant reactor power. Comparison shows that figures 2(b), 3(b), and 4(b) are identical (except for the limit boundaries) despite the different bleed-valves settings. The value of reactor power is not influenced by bleed-valves settings, only by the combination of chamber conditions and core-gas mass-flow rate. These parameters correspond to a value of fuel temperature, which in turn specifies $\delta k'_F$, which together with $\delta k'_W$ determines reactor flux and power.

Within the operating envelope in figure 2(b), reactor power varies from about 47 to nearly 120 percent of design. Furthermore, each curve of constant power fraction crosses the corresponding mass-flow fraction line at the 100-percent design value of chamber temperature. This fact is explained readily by considering the following energy equation:

$$\text{Power} = \dot{M}_c C_{P,c} \left(T_E - T_I\right)_c \tag{5}$$

At design core-gas exit temperature, or chamber temperature, the core-gas inlet temperature and specific heat are essentially constant. Therefore, reactor power and core-gas mass-flow rate assume the same fraction of their design values.

Poison reactivity. - The relative locations of the operating envelope boundaries in figure 2(c) indicate the amount of poison reactivity required for the system to function inside the operating region. The poison reactivity varies from 0 to about 1.5 dollars within this enclosure. The 100-percent design-point value is about 35 cents, which does not include any excess reactivity for xenon override. A variation in poison reactivity of about 2 dollars characterizes the region between heat-exchanger freezing and the pressure-tube temperature limit.

The curves of constant poison reactivity have a negative slope in figure 2(c). It would be desirable if they were vertical to simplify the controls. Then, if an operating

point was attained just above the pump stall line at a chamber temperature of 4460° R, the 100-percent design point could be reached by maintaining constant poison and merely closing the topping-turbine bypass valve. A positive slope might even be better; a point in the lower left area of the operating region would be a starting point for ascent to the 100-percent design point at constant poison reactivity. Nevertheless, knowledge of the location of the poison curves will be helpful in selecting an engine control system. Comparison of figures 2(c), 3(c), and 4(c) reveals a displacement of the constant poison reactivity curves to the left at the lower bleed-valves settings, so that less poison is required at a given chamber condition. The corresponding slopes in the graphite-reactor system are positive.

Water mass-flow rate. - The characteristics of the water mass-flow rate are presented in figure 2(d). Values in the operating region vary from about 75 to 105 percent of the design value, a much smaller range than the reactor-power variation. Furthermore, the relative flatness of the water mass-flow rate curves in figure 2(d) indicates that this parameter is insensitive to variations in chamber temperature.

Comparison of figures 2(d), 3(d), and 4(d) shows an upward displacement of the water mass-flow curves as the bleed-valves settings are lowered. This fact occurs because when the water-pump turbine throttle valve opening is reduced, the water-pump speed decreases; thus, the water mass-flow rate at any given point on the background map is lowered.

Mixed-mean water temperature. - Figure 2(e) presents curves of mixed-mean water temperature at the reactor exit. Within the operating region, this parameter varies from 620° to 720° R, approximately. The water system is pressurized to prevent boiling.

Comparison of figures 2(b), (d), and (e) shows that, as reactor power rises, both water mass-flow rate and water-temperature level rise. The rise in power is accompanied by rising water-pump turbine-inlet temperature T_1, which causes the rotational speed of this turbine to increase. Therefore, the water mass-flow rate rises. With rising reactor power, the bleed-pump turbine speed also increases, so that total hydrogen mass-flow rate rises.

In the heat exchanger, the transfer of heat from the hot water to the cold hydrogen is increased by the rises in the mass-flow rate of both fluids. Therefore, in the heat exchanger there is a tendency toward decreased water temperature as a result of the increased fluid mass-flow rates caused by the power rise.

Meanwhile, the rise in reactor power produces an increased heat input to the water in the core and the reflector. In addition, heat transfer from the pressure tube and reflector material is enhanced by the increased water mass-flow rate. Thus, in the reactor, the rise in power has a tendency to increase the water-temperature level.

Within the operating range, the water mass-flow rate is maintained at a relatively high level, varying from 75 to 105 percent of design (fig. 2(d)), while the reactor power

varies from 47 to 118 percent (fig. 2(b)). The high level maintained in the water mass-flow rate decreases the effects on the water in the heat exchanger and reactor. The two opposing tendencies in the heat exchanger and reactor account for the small change in water temperature experienced within the operating region. This explains why the water temperature rises only about 100° R when the reactor power level is raised from 47 to 118 percent of design.

Percent bleed. - The variation in percent bleed is presented in figure 2(f). For 100-percent design-point operation, almost 2.6-percent bleed is required. Within the operating region, this parameter varies from less than 2.5 to approximately 2.8 percent. The percent bleed rises with decreasing total hydrogen mass-flow rate because the constant bleed-valves settings force the bleed system to pass more hydrogen gas than is needed at low system mass-flow rates.

This trend of rising percent bleed with decreasing system flow rate also acts to maintain the variation in water mass-flow rate and temperature level in the small range previously noted. As reactor power is decreased, the greater-than-required percent bleed causes the water-pump turbine to rotate faster than required. Therefore, the water mass-flow rate is maintained at a higher value, and, although the water-temperature level is lowered because of the power decrease, the drop is small because of the favorable heat-transfer conditions in the reactor.

A similar situation occurs when the corresponding plots for the 60- and 36.6-percent bleed-valves settings are considered. Figures 3(f) and 4(f) show that at the 100-percent design point approximately 2.3 and 2.0 percent bleed occur, respectively. In these instances, the bleed-valves openings are closed more than required for high-power operation. The decrease in percent bleed at any point (such as the 100-percent design point) results in higher bleed-gas temperature. This explains why the curve of limiting water-pump turbine-inlet temperature moves into the operating corridors (see figs. 2(a), 3(a), and 4(a)) as the bleed-valves settings are changed progressively from the 100 to 60 to 36.6 percent settings.

Because of choking in the bleed valves, it is not necessary to control the bleed-gas mass-flow rate. With constant bleed-valves settings, the variation in percent bleed is small. A feature of the bleed system is its self-regulating characteristic: when hydrogen mass-flow rate is decreased, the percent bleed increases. This fact is also indicated by the negative slope of the water-pump turbine-inlet temperature constraint in figures 2(a), 3(a), and 4(a). This adds to the safety of bleed fuel-element operation. There is a slight penalty incurred, however, in the reduction in turbine energy available at low hydrogen mass-flow rates.

Topping-turbine bypass valve setting. - During the mapping survey, the position of the topping-turbine bypass valve was recorded. From this information, lines of constant valve setting are presented in figure 2(g), with the value at the 100-percent design point

as a base. These lines are similar to the core-gas mass-flow rate lines, except that their slopes are steeper. Their dissimilarity is due to two main factors: friction in core gas and topping-turbine inefficiency. The curves of constant valve setting and mass-flow rate are most dissimilar at the high-flow region in figure 2(g). In this region, the topping-turbine efficiency is close to its design value; thus, this factor has a small effect. However, the friction pressure drop, which is proportional to $\dot{M}_c^2$, is high so that the valve opening is increased over that required for frictionless flow. In the lower regions of figure 2(g), a low turbine efficiency resulting from far-off-design turbine operation is a major factor. Frictional pressure drop has a smaller effect here.

Along a line of constant $\dot{M}_c$ in figure 2(g), increasing chamber temperature requires opening the topping-turbine bypass valve, and closing the valve is accompanied by decreasing temperature. This means that at constant core-gas mass-flow rate the topping turbine develops a smaller share of the total work as chamber temperature is increased. Accordingly, the bleed-pump turbine produces a larger share of the work.

OPERATION AND CONTROL

In addition to defining the boundaries of feasible system operation, an objective of this study was to explore the system operation and control characteristics. The mapping surveys were conducted with the use of fixed bleed-valves settings to determine if this simplification in control could be used over a wide operating range. Figure 2(b) shows that this is possible above approximately 47 percent of reactor power with the use of the 100-percent bleed-valves settings. Of the six manipulated variables for control listed on page 6, this simplification requires that only two, poison reactivity and topping-turbine bypass valve, be adjusted for maneuvers within the operating envelope of the map given in figure 2(a).

On the other hand, the severely restrictive confines of the operating corridor in figure 5 indicate that simplification in control may not be a valid objective. Because maneuvers within this envelope are so limited, it may be advisable to monitor the various damage limits and provide the capability to override the main control parameters. In doing so, however, measuring such parameters as nozzle-wall temperature accurately may introduce a major problem.

Since these practical considerations have been recognized, this report discusses the theoretical aspects in further simplifying system control. The ultimate simplification would arise if the need for controlling either poison reactivity or the topping-turbine bypass valve could be eliminated. Thus, it would be highly desirable to control system operation by the topping-turbine bypass valve alone. The nonfeasibility of this procedure

is readily displayed by considering figure 2(c). From the 100-percent design point if constant poison reactivity is maintained, a maneuver involving opening the topping-turbine bypass valve results shortly in overheating the nozzle wall. The reverse procedure started from a lower point steers the system toward heat-exchanger icing. The negative slopes of the constant poison reactivity curves prevent this simplification.

On the other hand, figure 2(g) reveals that fixing the topping-turbine bypass valve setting to attempt operating maneuvers on the map by adjusting poison reactivity alone is also in vain. Thus, with only one control, it is impossible to operate the system within the feasible operating region. A minimum of two control variables is required.

Possible Operating Paths

This discussion implies that two control parameters are required for maneuvers within the feasible operating envelope. Possible use of parameters other than poison reactivity and topping-turbine bypass valve is discussed in the next section. For the present, however, a simple path employing both of these control parameters is considered. Possible modifications to the system that would permit startup and acceleration through the low-power region to the 100-percent design point are disscussed in the section SUGGESTED MODIFICATIONS. It is suggested that this method be used to attain a point within the operating capability of the preliminary reference system with the

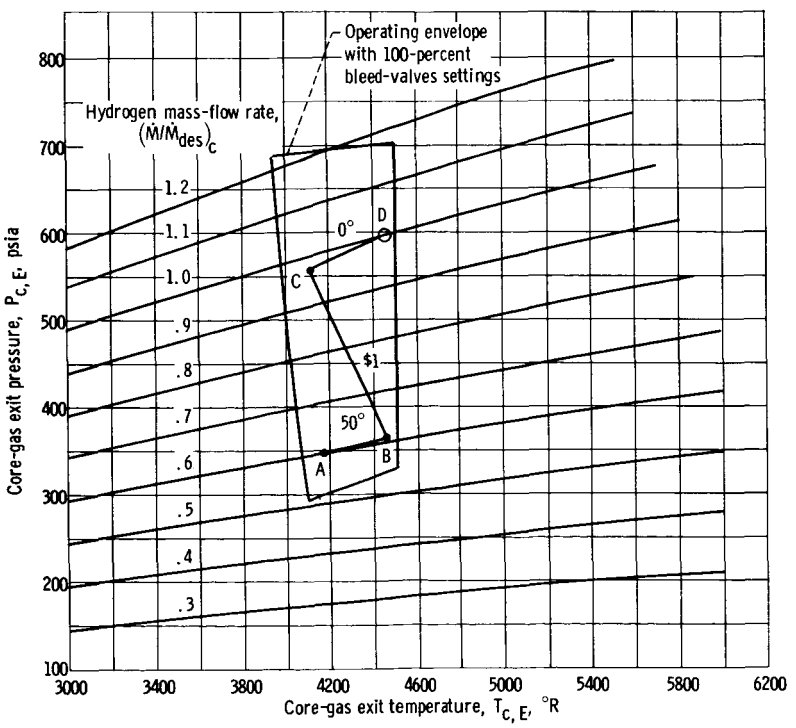

Figure 6. - Suggested operating path for tungsten water-moderated reactor system.

100-percent valves settings. Such a point is designated point A in figure 6 and on overlay 4, which will be helpful in illustrating a path from A to the 100-percent design point D: Figure 6 consists of a background map of hydrogen mass-flow rate curves, a superimposed operating region for 100-percent bleed-valves settings, and a suggested operating path taken from figures 2(c) and (g). Overlay 4 can be used with these two figures. At point A, the heat-exchanger splitter valve of the modified reference system can be closed, and regulation of the bleed-pump-turbine throttle and bypass valves can be discontinued by setting them at the 100-percent positions. The modified reference system therefore reverts to the preliminary reference system.

Point A is characterized by the following system parameters:

$$\frac{\text{Power}}{\text{Design power}} = 0.56$$

$$T_{c,E} = 4180^{\circ}\ R$$

$$\delta k'_p = \$1.35$$

$$\left(\theta - \theta_{des}\right)_5 = 50^{\circ}$$

If this topping-turbine bypass valve setting is maintained constant while the poison reactivity is reduced to 1 dollar, point B is reached. Thereupon, this valve can be closed down to the 100-percent design-point setting while the poison reactivity is kept at 1 dollar. This establishes point C. The 100-percent design point D is now accessible by decreasing the poison while keeping the topping-turbine bypass valve setting fixed at the 100-percent design position. The path ABCD is also included on the composite map (fig. 5, p. 28) so that the changes in reactor power and hydrogen mass-flow rate can be shown. From B to C, the reactor power rises from 60 to 90 percent of design, while the mass-flow rate rises from 60 to 97 percent.

Thus, for path ABCD only two controls are needed, poison reactivity and topping-turbine bypass valve, only one of which is operated at a time. Of course, a more direct path from A to D is possible by controlling both of these parameters simultaneously. Furthermore, many alternate paths are possible within the limited operating envelope. If the constant poison reactivity curves had a positive slope, it might be possible to proceed directly from A to D. Further study is required to determine if changes to the system design could yield a vertical or positive slope.

From point B to C, the chamber temperature decreased from a value of 4450° to 4120° R. If this drop should be judged unacceptable from the standpoints of vehicle performance or fuel-temperature considerations, constant-temperature paths such as A to C or B to D could be programed.

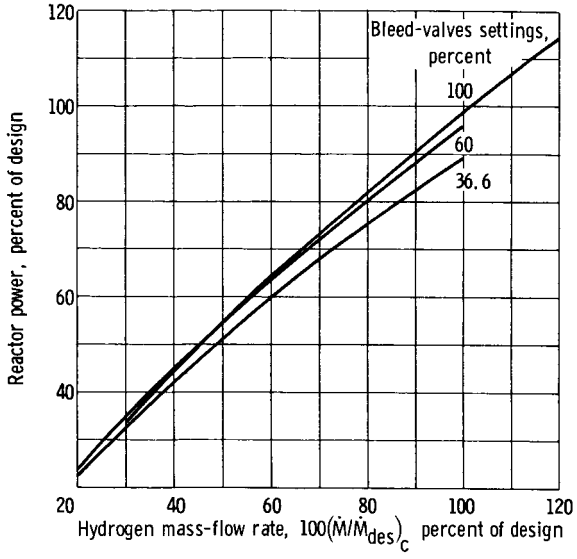

Figure 7. - Variation in reactor power with hydrogen mass-flow rate at constant poison reactivity of 50 cents.

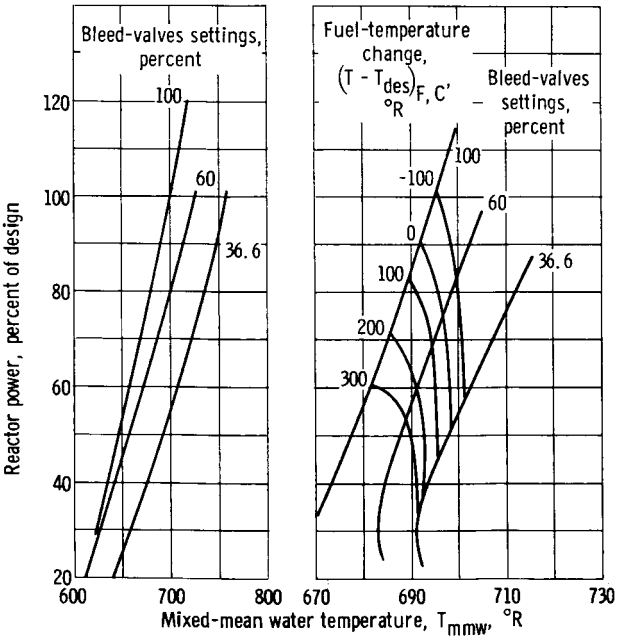

(a) Core-gas exit temperature, 4460° R.

(b) Constant poison reactivity, 50 cents.

Figure 8. - Variation in reactor power with mixed-mean water temperature.

Possible Control Parameters

Hydrogen mass-flow rate. - In the search for a parameter suitable for a reactor power controller, the hydrogen mass-flow rate was considered. For this purpose reactor power was plotted in figure 7 against hydrogen mass-flow rate, with poison reactivity maintained constant at 50 cents for the three bleed-valves settings. Use of a 50-cent poison reactivity in figure 7 accounts for the fact that slightly less than 100-percent design reactor power is indicated at 100-percent of design mass-flow rate. As was mentioned previously, the poison reactivity at the 100-percent design point is about 35 cents (see fig. 2(c), p. 16). Figure 7 shows that reactor power is nearly proportional to hydrogen mass-flow rate. This relation is also true if chamber temperature is kept constant instead of poison reactivity (fig. 2(b), p. 15). Therefore, the topping-turbine bypass valve, through its effect on the hydrogen mass-flow rate, appears promising as a parameter to control reactor power. Because engine thrust is also proportional to hydrogen mass-flow rate, its effect on engine thrust must also be considered.

Water temperature. - When this reactor system was conceived, it was anticipated that water temperature might be used to control reactor power. For example, the low temperature of the water could be sensed more easily than hot-gas temperature. Figure 8 was plotted to explore this possibility. In figure 8(a), relative reactor power is plotted against

mixed-mean water temperature at design chamber temperature for all three bleed-valves settings. The steep slopes of the curves in this figure reflect the previously mentioned small change in water temperature accompanying large changes in reactor power. Figure 8(a) indicates that, when the reactor power changes 1 percent of the design value, the water temperature changes about 1° R for the 100-percent bleed-valves settings. For the other two bleed-valves settings, the power change is about 0.7 percent per $^{\circ}$R.

Figure 8(b) is similar to figure 8(a) except that poison reactivity is maintained constant at a value of 50 cents, and, therefore, chamber temperature varies. Also plotted in figure 8(b) are curves of constant fuel temperature change to aid in displaying the feedback reactivity characteristics of the system. Under the condition of constant poison reactivity, less than a 3-percent change in reactor power is accompanied by a 1° R change in water temperature. Therefore, controlling reactor power by sensing water temperature during either constant temperature or constant poison operation appears feasible.

Figure 8(b) shows that along any of the curves of constant bleed-valves settings the water temperature and reactor power both rise (or drop) together; that is, the slopes of the curves are positive. That this is not a paradox, as it might seem from the negative water-temperature reactivity of the system, is shown by considering the relative locations of the constant fuel-temperature change curves. As reactor power is increased along a curve of constant bleed-valves settings in figure 8(b), the fuel-temperature level decreases. This decrease in fuel temperature causes an increase in the fuel reactivity $\delta k'_F$ (see eq. (D178)), which tends to raise reactor power. At the same time, the decrease in $\delta k'_W$ in response to the increase in water temperature tends to lower the reactor power level. Under the condition of constant poison reactivity in figure 8(b), the resulting reactivity is determined by $\delta k'_F$ and $\delta k'_W$ (see eq. (D176)) only. The positive slopes shown in figure 8(b) imply that the effect of $\delta k'_F$ is dominant under these conditions. This observation follows from the fact that, when the fuel temperature drops 200° R, in figure 8(b), the water temperature rises only 6° or 7° R.

The constant fuel-temperature change curves in figure 8(b) provide further insight in understanding the behavior of the system with respect to temperature-reactivity feedbacks. Because poison reactivity is maintained constant throughout figure 8(b), the curves of constant fuel-temperature change isolate the effect of the water-temperature reactivity on reactor power. Equation (D178) shows that, if fuel temperature is constant, $\delta k'_F$ is constant. Therefore, in accordance with equation (D176), $\delta k'_W$ alone is responsible for the reactor power variation along the curves of constant fuel-temperature change. Thus, from the curve representing 100-percent bleed-valves settings if the system is operated to maintain constant fuel temperature, figure 8(b) discloses that the water temperature rises. The concomitant decrease in $\delta k'_W$ results in a drop in reactor power. This hypothetical manner of operating the system necessitates changes in the bleed-valves settings.

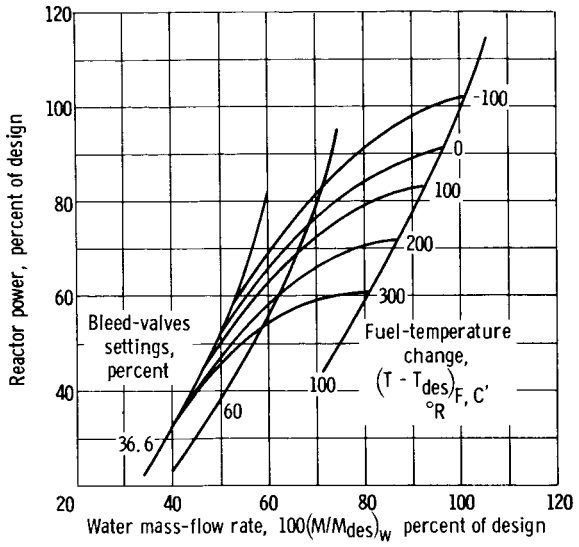

Figure 9. - Variation in reactor power with water mass-flow rate at constant poison reactivity of 50 cents.

The negative slopes of the constant fuel-temperature change curves reflect the negative characteristic of the water-temperature reactivity. The steepness of the slopes illustrates the high sensitivity of reactor power to this parameter. The safety aspect inherent in this reactor design concept is shown clearly by the fact that the slopes of the constant fuel-temperature change curves become steeper with increasing water temperature.

Water mass-flow rate. - Figure 9 is a cross plot made to present the effect of water mass-flow rate on reactor power when poison reactivity is maintained at 50 cents. Once again, curves of constant fuel-temperature change are included to enhance the understanding of interactions caused by temperature-reactivity feedbacks. At the 100-percent bleed-valves settings, a 2-percent change in reactor power is accompanied by a 1-percent change in water mass-flow rate. The sensitivity of water mass-flow rate to reactor power variation implies that sensing this flow rate might be employed for reactor-power control. Other factors, however, outweigh this characteristic. Water mass-flow rate should be maintained at a high level to alleviate the possibility of heat-exchanger icing and to provide an extra margin from the pressure-tube temperature limit. Furthermore, a high water mass-flow rate is indicative of a fast water-loop response time, which is desirable because it increases the temperature coupling of the hydrogen and the water.

Figure 9 shows that along any curve representing constant bleed-valves settings and with constant poison reactivity, water mass-flow rate rises when reactor power rises. The water mass-flow rate rises despite a drop in percent bleed (fig. 2(f)). This drop is small so that the large increase in total hydrogen mass-flow rate (fig. 2(c)) results in a rise in bleed-gas mass-flow rate and, hence, a rise in water-pump turbine energy. The increase in water mass-flow rate results in raising the water-temperature level but only by a small amount, as explained in the discussion of the opposing effects in the heat-exchanger and reactor. Finally, as discussed in connection with figure 8(b), the effect of the small water-temperature rise is outweighed by the 200° R drop in fuel-temperature so that a net rise in reactor power is experienced.

As in figure 8(b), the constant fuel-temperature change curves in figure 9 isolate the effect of the water. In this instance, however, the effect is interpreted in terms of water mass-flow rate because of its use as the abscissa in figure 9. The positive slopes of the curves of constant fuel-temperature change (fig. 9) show that reducing the bleed-valves

settings results in decreased water mass-flow rate and reactor power. In the same hypothetical mode of operation, figure 8(b) indicates that the water temperature rises. This rise accounts for the observation in figure 9 that reactor power decreases along a constant fuel-temperature change curve as the bleed-valves settings are reduced.

Poison reactivity. - Comparison of figures 2(c) and (e) reveals that the slopes of the constant poison reactivity and water-temperature curves at any given point are similar. The slopes of the former curves are somewhat steeper, however. The similarity is not surprising when it is recalled that constant fuel-temperature curves are nearly vertical in figure 2(a). This characteristic lessens the comparative effect of $\delta k'_F$ on the curves of figures 2(c) and (e). Thus, because the net reactivity is zero in steady-state operation, equation (D176) implies that $\delta k'_p$ and $\delta k'_w$ tend to offset each other. That is, the constant poison-reactivity curves are a direct reflection of the water-temperature reactivity, which, in turn, follows the water temperature.

The results implied in the foregoing discussion are verified by figure 10, which shows the variation in reactor power with poison reactivity when chamber temperature is maintained at 4460° R. Because the poison reactivity is essentially the negative of the water reactivity at constant chamber temperature, figure 10 is approximately a mirror image of figure 8(a). The lack of exact correspondence lies in the fact that the fuel reactivity varies slightly along each of the curves. As in figure 8(a), the steepest slope occurs with 100-percent bleed-valves settings. At the latter settings, insertion of 10 cents of poison results in a decrease of about 7 percent in the design power. Furthermore, with poison insertion there is a transient tendency to undershoot both reactor power and core-gas exit temperature.

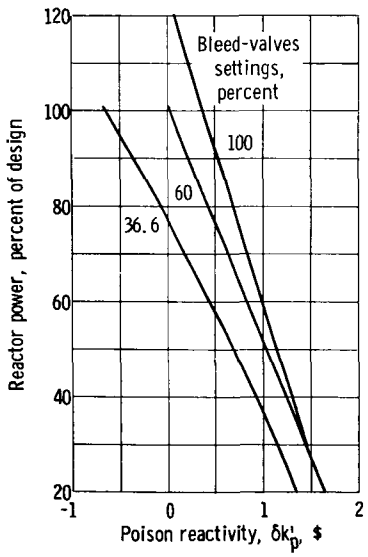

Figure 10. - Variation in reactor power with poison reactivity at design chamber temperature of 4460° R.

The extreme sensitivity of reactor power to poison reactivity requires that reactor power be accurately sensed and that poison reactivity be minutely controlled for operational maneuvers, such as path ABCD in figure 5. In the modifications to be discussed subsequently, it was found that the heat-exchanger splitter valve was suitable for control of reactor power. If it should be found that finer control is available from manipulation of this valve, once point A in figure 5 is reached by the modified reference system, to reach point D it may be desirable to make the appropriate changes in reactor power by adjusting the heat-exchanger splitter valve instead of the poison reactivity. Furthermore, the tendency of poison insertion to cause transient temperature undershoots would be replaced by a smoother transient resulting from the transport delay in the water loop. Performance obtained by adjusting the heat-exchanger splitter

valve with constant poison reactivity would approximate that using water temperature as a controller.

Bleed-Valves Considerations

It has been shown that the threshold of bleed-pump stall recedes to a lower hydrogen mass-flow rate as the bleed-pump-turbine throttle valve setting is reduced to satisfy the requirements of a 2-to-1 power split between the topping and bleed pumps. This observation indicates that fixing the bleed-pump-turbine throttle valve at a minimum setting would yield the lowest stall condition. Then, since the system tends to unload the bleed pump as mass-flow rate and power rise, the bleed-pump power fraction would be at a minimum at the 100-percent point. Because of the nature of pumps in series, the topping pump assumes the load fraction dropped by the bleed pump and thus causes the former to approach stall. There evidently exists a problem of optimizing the fixed bleed-pump-turbine throttle valve setting to accommodate the stall limits of both pumps. It does not appear necessary to control the pump work split in the steady-state range above 47 percent of design reactor power because of the absence of stall above this level.

Because of the trend for the bleed pump to increase its load fraction as flow and power decrease, it appears that this pump would carry the full load at startup. Reference 5 corroborates this expectation which, however, cannot materialize because of the pump stall characteristic. Thus the topping pump must carry a share of the load. Therefore, a control would be required to maintain a suitable, varying power split during startup. An alternate scheme would be to provide a control to maintain operation of both pumps with equal margins from stall, as was done in references 5 and 6.

A high water mass-flow rate is desirable to avoid heat-exchanger freezing and for decreasing the water-loop response time. Therefore, it is concluded that both the water-pump-turbine throttle and bypass valves can be replaced by orifices sized at the 100-percent conditions for use over the operating range of this investigation. Sizing the orifices at the 100-percent conditions would provide adequate water mass-flow rate and would prevent the water-pump-turbine-inlet temperature limit being reached at low reactor power levels.

The bleed-pump-turbine throttle and bypass valves cannot be replaced by orifices for operation below about 47 percent of design reactor power if they are set to yield a 2-to-1 pump work split at the 100-percent design point because of bleed-pump stall. With the heat-exchanger bypass configuration, these two valves require continuous manipulation to permit startup and acceleration through the low-power range.

SUGGESTED MODIFICATIONS

It is evident from figure 5 (p. 28) that improvement in performance of the preliminary reference system requires that the operating envelope be opened to encompass a wider range and extended to allow low-power operation. The location of the high-power side of the operating corridor is considered critical because although it does not theoretically restrict design-chamber-temperature operation, it may not provide an adequate margin from the nozzle-wall temperature limit. Movement of this and the successive boundaries would require relaxing the nozzle wall, fuel, and water-pump turbine-inlet temperature limits or changing the design of the nozzle and the main bleed fuel elements.

Widening the operating region also involves finding a means of overcoming the heat-exchanger freezing problem to allow removal or displacement of this boundary on the map of figure 5. To do so requires reducing the water-temperature drop in the heat exchanger. The drop in water temperature can be reduced by increasing the water mass-flow rate, decreasing the exchanger surface area, or decreasing the hydrogen mass-flow rate through the heat exchanger. Raising the water mass-flow rate would be ineffective for this purpose, however, because of the opposing effects in the reactor and heat exchanger on water-temperature level. Reducing the heat-exchanger surface area enough to be effective would cause the pressure-tube temperature limit to be exceeded because of inadequate cooling. Decreasing the hydrogen mass-flow rate in the heat exchanger also tends to promote excessive pressure-tube temperature because of the resultant higher heat-exchanger water-exit temperature. This scheme, however, has the advantage of being controllable. A portion of the main hydrogen mass flow can be bypassed around the heat exchanger, the amount being regulated by a valve.

This discussion implies that heat-exchanger icing and a pressure-tube temperature limit are fundamental limits in the water system. Any modification selected must provide a compromise that constrains the water system to operate between these two limits.

Extending the operating envelope farther into the low-power region requires lessening the load on the bleed pump to keep it out of stall. Programing control of the bleed valves to maintain both bleed and topping pumps equidistant from stall is a possibility. Decreasing the hydrogen system pressure drop, or impedance, is another. This could be accomplished by bypassing some of the hydrogen around the nozzle-coolant tubes, which form a high-pressure drop component.

In accordance with these considerations, three particular modifications to the preliminary reference system were selected for further study. This work is reported in references 5 and 6.

In one modification, the preliminary reference system was altered to include hydrogen bypass around the heat-exchanger with a splitter valve at the exit. It was shown that this modification successfully enlarged the operating region and extended low-power

operation down to about 13 percent of design reactor power. A second modification included nozzle-coolant tube bypass in addition to the heat-exchanger bypass. This modification was inferior to the preliminary reference system in high-power performance. Emergence of the nozzle-coolant temperature-limit constraint prevented design chamber-temperature operation over the entire range below the 100-percent design point. The third modification studied was an all-topping cycle with heat-exchanger hydrogen bypass. Besides achieving virtually the same performance improvement as the first modification, this design also simplified controls and system complexity by elimination of the bleed system.

From the results of references 5 and 6, it appears that system startup would be possible by using any of these modifications. The all-topping cycle is ideal from the standpoint of requiring control of only the topping-turbine and heat-exchanger bypass valves. The topping cycle, however, appears to have limited growth potential for developing the high chamber pressures anticipated for use with advanced nozzle designs. This limitation arises from the inability of the topping cycle to supply the turbine with enough energy to meet increased demands in turbine power within the existing core design. The modification using heat-exchanger bypass also has startup capability, but requires continuous regulation of the bleed-pump-turbine throttle and bypass valves to maintain both hydrogen pumps at equal margins from stall. This modification does, however, allow replacement of the water-pump-turbine throttle and bypass valves by fixed orifices. The heat-exchanger bypass modification was therefore chosen for more extensive study. With regard to the preliminary reference system again, it may be possible to preheat the water to permit chilldown and startup without heat-exchanger icing.

As a consequence of results obtained from the study of the preliminary reference system, a simple modification to the design incorporating a cold-hydrogen bypass around the heat-exchanger was investigated in references 5 and 6. Some of the conclusions made by references 5 and 6 pertaining to the modified reference system are as follows:

(1) The operating corridor was opened considerably, and a limit on the pressure-tube temperature replaced heat-exchanger freezing as the low chamber-temperature boundary.

(2) Startup appears feasible, because the steady-state pump-stall-pressure-tube temperature-limit intersection was lowered to about 13 percent of design reactor power.

(3) Control of the heat-exchanger splitter valve can function as an alternate or supplement to poison reactivity.

CONCLUSIONS

The steady-state analog simulation of the tungsten water-moderated reactor preliminary reference system led to many conclusions. Some of the more significant conclusions are as follows:

1. The system appears stable without external feedback controls.

2. A lower limit to steady-state operation is imposed by the simultaneous occurrence of heat-exchanger icing and bleed-pump stall. This occurs at about 35 percent of design hydrogen mass-flow rate and 33 percent of design reactor power.

3. Although the steady-state results indicate that the preliminary reference system may encounter severe problems in startup, conclusive evidence would require a low-power transient investigation.

4. High-power operation is limited by bleed-pump turbine rotational speed.

5. As chamber temperature is increased, the system encounters successive temperature limits in the following components: nozzle-wall, fuel, water-pump turbine-inlet, and pressure-tube.

6. Reactor power can be controlled by two parameters: the topping-turbine bypass valve and poison reactivity. As an alternative, water temperature is a suitable control parameter.

7. In a search for parameters suitable for reactor control, the following relations were found: reactor power is approximately proportional to hydrogen flow rate; a poison reactivity insertion of 10 cents reduces reactor power by about 7 percent; and less than a 3-percent change in reactor power is accompanied by a 1^{o} R change in water-temperature level.

8. The water mass-flow rate should be maintained at a high level; therefore, the water-pump-turbine throttle and bypass valves can be replaced by fixed orifices sized for 100 percent design-point operation.

9. Reactor power and hydrogen mass-flow rate are not influenced by pump work split or the positions of the valves in the bleed system.

10. In the operating range above 47 percent of design reactor power, system control can be simplified by maintaining the bleed-pump-turbine valves at their 100-percent positions. In this region, operation can be controlled by the topping-turbine bypass valve and poison reactivity, only.

11. As reactor power is reduced with constant bleed-valves settings, the bleed pump assumes an increased fraction of the load causing this pump to approach stall. Below 47 percent of design reactor power, the pump work split must be adjusted to keep the bleed pump out of stall.

12. The bleed-gas mass-flow rate does not require control in the range of this study. There is a self-regulating tendency in which the percent bleed rises as reactor power and total hydrogen mass flow rate are decreased.

13. Design chamber temperature (or specific impulse) is potentially obtainable at all reactor power levels above about 37 percent of design, at which point bleed-pump stall occurs. The margin from the nozzle-wall temperature limit, however, is very small.

14. The settings of the valves in the bleed system determine the locations of all system constraints on a steady-state map, except the nozzle-wall and fuel-temperature limits.

Lewis Research Center,
National Aeronautics and Space Administration,
Cleveland, Ohio, September 15, 1966,
122-28-02-04-22.

APPENDIX A

SYMBOLS

A	area, ft^2
BTBV	bleed-pump-turbine bypass valve
BTTV	bleed-pump-turbine throttle valve
b	hydrogen temperature-ratio factor in expression for convection heat-transfer coefficient
$C_{i'}$	concentration of delayed-neutron precursors of i'^{th} group, nuclei/ft^3
C_P	specific heat at constant pressure, Btu/(lb mass)(^oR)
C_V	specific heat at constant volume, Btu/(lb mass)(^oR)
c_v	valve flow-capacity coefficient
D	hydraulic diameter, ft
E	thermodynamic internal energy, Btu/lb mass
e	total internal energy, Btu/lb mass
F'	mass-flow function set on variable diode function generator
f	friction factor
f'	pressure-ratio function set on variable diode function generator
f''	water-temperature reactivity function set on variable diode function generator
G	factor in expression for heat-transfer coefficient
G'	pump pressure-speed function set on variable diode function generator
g	acceleration of gravity, ft/sec^2
g'	pump torque-speed function set on variable diode function generator
H	factor in expression for convection heat-transfer coefficient
h	convection heat-transfer coefficient, Btu/(ft^2)(sec)(^oR)
I	turbopump moment of inertia, lb mass (ft)(sec^2)
J	mechanical equivalent of heat, (ft)(lb mass)/Btu
K, K_1, K_2	constants
k	thermal conductivity, Btu/(ft)(sec)(^oR)
k'	reactivity
L	torque, (lb force)(ft)
ℓ^*	mean lifetime of neutrons, sec

$\dot{M}$	mass-flow rate, lb mass/sec
N	rotational speed, rpm
n	neutron density, neutrons/ft^3
P	absolute pressure, lb force/ft^2
$\dot{Q}$	heat generation rate, Btu/sec
R	gas constant for hydrogen, (ft)(lb force)/(lb mass)(^oR)
Re	Reynolds number
S	general heat-flow rate, including generation and convection, Btu/sec
s	Laplace transform variable
T	absolute temperature, ^oR
TTBV	topping-turbine bypass valve
t	time, sec
u	fluid velocity, ft/sec
V	volume, ft^3
WTBV	water-pump-turbine bypass valve
WTTV	water-pump-turbine throttle valve
x	axial distance, ft
y	radial distance, ft
Z	constant entrance-exit loss factor in expression for friction factor
z	distance in plane normal to both x and y, ft
β	sum, for all groups, of fractions of fission neutrons that are delayed neutrons
$\beta_{i'}$	fraction of fission neutrons that are delayed neutrons in i'^{th} group
γ	ratio of specific heats for hydrogen gas, C_P/C_V
ϵ	error between demand and calculated values
θ	topping-turbine bypass valve angle, deg
$\lambda_{i'}$	decay constant of delayed-neutron precursors of i'^{th} group, sec^{-1}
μ	absolute viscosity, lb mass/ft-sec
ρ	mass density, lb mass/ft^3

Subscripts:

A	upstream axial section in three-section model
B	middle axial section in three-section model
B, E	bleed exit
BF	bleed fuel
BG	bleed gas
BN	bleed nozzle
BP	bleed pump
BT	bleed-pump turbine
BTP	bleed turbopump
b	bulk
C	downstream axial section in three-section model
CN	coolant nozzle

CNW	coolant-nozzle wall
c	hydrogen in core
D	flow-divider tube
des	design
E	exit
F	fuel
f	film
fr	friction
H	hydrogen-side surface in heat exchanger
He	heat exchanger
I	inlet
i	inner
i'	index representing energy group of delayed neutrons
$\dot{M}$	mass-flow rate
max	maximum
mmw	mixed mean water
N	nozzle hot-gas side
o	outer
P	pump
PT	pressure tube
p	poison
R	side reflector
ref	reference
S	surface
SH	stagnant hydrogen
T	temperature
TOT	total
TP	topping pump
TT	topping turbine
TTP	topping turbopump
W	water-side surface in heat exchanger
WP	water pump
WT	water-pump turbine
WTP	water turbopump
w	water in reactor
X	hydrogen in heat exchanger
x	water in heat exchanger
1	water-pump-turbine throttle valve
2	water-pump-turbine bypass valve
3	bleed-pump-turbine throttle valve
4	bleed-pump-turbine bypass valve
5	topping-turbine bypass valve
1'	inlet axial station
2'	axial station at interface between sections A and B
3'	axial station at interface between sections B and C

APPENDIX B

ASSUMPTIONS

The following assumptions were used in the analysis:

General:

(1) Flow through piping is adiabatic.

(2) Temperature transport lags in piping are negligible.

(3) Radiation heat transfer to the pressure tubes from the tungsten support tubes is included in the term for conduction through the stagnant hydrogen.

(4) Gamma and neutron heating rates are proportional to reactor power level.

(5) Radial temperature gradients in the fuel, pressure tubes, and flow dividers are negligible.

(6) Heat loss entering the pressure tubes through the stagnant hydrogen is a linear function of the reactor power.

(7) Friction factors are constants, but a different constant is used with each set of bleed-valves settings.

Hydrogen Flow System:

(1) Flow through both hydrogen pumps is liquid, and density is constant in each pump.

(2) Hydrogen gas is treated as a perfect gas.

(3) Gas properties in the core, bleed, and heat exchanger are constants but have a different (iterated) value in each axial section.

(4) The many core, bleed, and heat-exchanger gas flow passages are each represented by a single equivalent passage.

(5) Gamma and neutron heating in the hydrogen are negligible.

(6) Gas axial pressure variation in the core and heat exchanger is linear.

(7) The thrust and bleed nozzles and the bleed-pump-turbine bypass valve are always choked. The topping-turbine bypass valve is never choked.

(8) The total temperature is constant across each valve.

(9) The thrust-nozzle chamber temperature equals the core-gas exit temperature.

(10) The nozzle coolant-tube wall temperature is proportional to the core-gas exit temperature.

(11) The core-gas inlet temperature is proportional to the heat-exchanger exit temperature.

(12) Water-pump and bleed-pump turbine exit temperatures are proportional to the bleed-gas exit temperature.

(13) Heat-transfer from the radiation shield is proportional to the bleed-gas exit temperature.

(14) The bleed gas makes only one pass through the core.

(15) Inlet conditions to the bleed system are the same as to the main fuel elements.

(16) At each set of bleed-valves positions, turbine temperature ratios are assigned the constant values obtained from the corresponding reference point.

(17) Hydrogen flow through the nozzles is isentropic.

Fuel Assembly:

(1) One equivalent fuel cylinder represents the assembly of concentric fuel rings and annular coolant passages in both the main core and bleed system.

(2) The neutron kinetics are space-independent and are simulated by a point model.

(3) Neutron kinetics in the bleed system is not simulated. The power generated in the bleed fuel elements is assumed proportional to the power produced by the main fuel elements.

(4) Reactivity feedbacks are represented as functions of weighted average core-gas and core-water temperatures.

(5) The contribution to reactivity of the hydrogen density is negligible.

Water Flow System:

(1) The temperature rise across the water pump is negligible.

(2) Heat transfer in the water plenums is negligible.

(3) The many water-flow passages in the reflector are simulated by a single equivalent passage.

(4) The fractions of total water flow rate passing through the side reflector and both inside and outside the flow-divider tubes are constants and equal to the 100-percent design values.

(5) Heat transfer from the bleed-assembly aluminum pressure tubes to the water is negligible.

Heat Exchanger:

(1) A single equivalent tube with surrounding water flow represents the shell-and-tube heat exchanger.

(2) Neutron and gamma heating in the heat-exchanger tubes and gas are neglected.

APPENDIX C

BASIC EQUATIONS

The three fundamental equations of fluid flow (continuity, momentum, and energy) are reviewed herein and presented in forms suitable for analog computation.

Continuity Equation

By considering a mass balance in a stationary volume element through which fluid is flowing, the author of reference 7 derived the familiar continuity equation

$$\frac{\partial \rho}{\partial t} = -\nabla \cdot (\rho u) \tag{C1}$$

In the present one-dimensional analysis, the form used is

$$\frac{\partial \rho}{\partial t} = -\frac{\partial}{\partial x}(\rho u) \tag{C2}$$

Momentum Equation

Newton's law of motion is applied in reference 7 to a fluid volume:

$$\frac{\partial(\rho u)}{\partial t} = -g\frac{\partial P}{\partial x} - \frac{\partial(\rho u^2)}{\partial x} \tag{C3}$$

or

$$\frac{\partial(\rho u)}{\partial t} = -g\frac{\partial P}{\partial x} + \frac{(\rho u)^2}{\rho^2}\frac{\partial \rho}{\partial x} - \frac{1}{\rho}\frac{\partial(\rho u)^2}{\partial x}$$

Preliminary analog transient runs revealed that the term $\partial(\rho u)^2/\partial x$ is negligible. Deleting this term and including additional terms to represent friction and sudden expansion and contraction yield

$$\frac{\partial(\rho u)}{\partial t} = -g\frac{\partial P}{\partial x} + \frac{(\rho u)^2}{\rho^2}\frac{\partial \rho}{\partial x} - \frac{2f(\rho u)^2}{\rho D} - K\frac{(\rho u)^2}{\rho} \tag{C4}$$

Energy Equation

The energy equation is derived by applying an energy balance to a control volume, such as that shown in figure 11(a):

Change of internal energy in volume = Net heat conducted in

+ Net heat convected in + Heat generated within

+ Net work done by pressure forces + Viscous dissipation

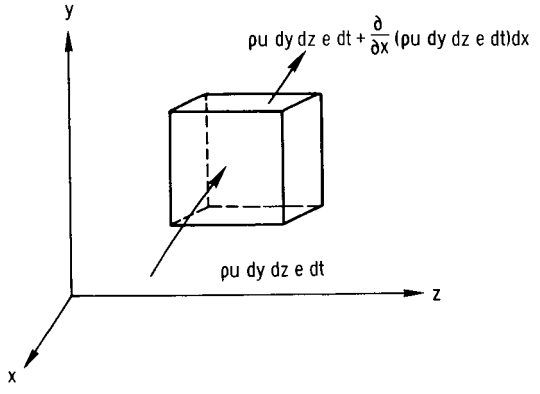

(a) Application of energy balance.

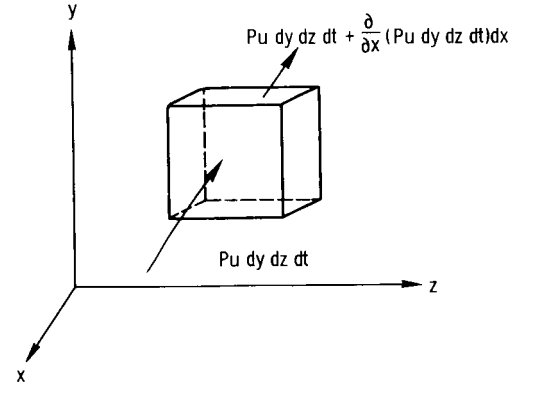

(b) Application of pressure forces.

Figure 11. - Control volume.

In this investigation, conduction within a flowing gas is neglected, as is viscous dissipation. The small magnitudes of these terms does not warrant the amount of analog equipment needed to simulate them.

The total internal energy per unit mass e is

$$e = E + \frac{u^2}{2gJ} \tag{C5}$$

where E is the thermodyanmic internal energy per unit mass, and $u^2/2gJ$ is the kinetic energy per unit mass. The net inflow of total internal energy occurring through the x-faces is

$$-\frac{\partial}{\partial x}(\rho u e)dx\ dy\ dz\ dt \tag{C6}$$

in time increment dt.

The net increase in internal energy within the control volume in time dt is

$$\frac{\partial}{\partial t}(e\rho)dx\ dy\ dz\ dt \tag{C7}$$

Consideration of the pressure forces on the x-faces, as in figure 11(b), leads to an expression for the net work done on the volume:

$$-\frac{1}{J}\frac{\partial}{\partial x}(Pu)dx\,dy\,dz\,dt \tag{C8}$$

If S is used to denote the sum of the heat-generation rate and heat-convection terms, the energy equation can be expressed as

$$-\frac{\partial(\rho ue)}{\partial x} - \frac{\partial(Pu)}{J\partial x} + \frac{S}{V} = \frac{\partial(e\rho)}{\partial t} \tag{C9}$$

With the use of equations (C2), (C3), and (C5), equation (C9) can be written in the form

$$\rho\left(\frac{\partial E}{\partial t} + u\frac{\partial E}{\partial x}\right) = \frac{S}{V} - \frac{P}{J}\frac{\partial u}{\partial x} \tag{C10}$$

In the notation of the total derivative

$$\frac{D}{Dt} = \frac{\partial}{\partial x}\frac{dx}{dt} + \frac{\partial}{\partial t} \tag{C11}$$

equation (C10) becomes

$$\rho\frac{DE}{Dt} = \frac{S}{V} - \frac{P}{J}\frac{\partial u}{\partial x} \tag{C12}$$

Equation (C12) applies to flow in a constant area passage. If the flow area varies, the counterpart of equation (C12) is

$$\rho A\frac{DE}{Dt} = \frac{S}{V} - \frac{P}{J}\frac{\partial(uA)}{\partial x} \tag{C13}$$

as is shown in reference 7.

For an ideal gas

$$E = \int C_V\,dT + \text{const}$$

$$= C_V T + \text{const} \tag{C14}$$

where C_V is assumed constant. Therefore, from equations (C12) and (C14),

$$\rho C_V \frac{DT}{Dt} = \frac{S}{V} - \frac{P}{J} \frac{\partial u}{\partial x} \tag{C15}$$

With the use of the equation of state for a perfect gas,

$$P = \rho RT \tag{C16}$$

and the continuity equation (eq. (C2)), equation (C15) can be written as

$$\rho C_P \frac{DT}{Dt} - \frac{1}{J} \frac{DP}{Dt} = \frac{S}{V} \tag{C17}$$

Checkout transient analog runs revealed that omission of the term DP/Dt had a negligible effect. Therefore, when equation (C17) is expanded by equation (C11), it becomes

$$\frac{\partial T}{\partial t} = -u \frac{\partial T}{\partial x} + \frac{S}{\rho C_P V} \tag{C18}$$

APPENDIX D

APPLICATION OF BASIC EQUATIONS

In this appendix the fundamental equations are applied to the components used in the model. All equations programed in the simulation are presented herein in the form used. Stations and nomenclature are indicated in figure 1 (p. 4). Hydrogen properties used in the analysis were taken from reference 8.

HEAT EXCHANGER

Water Energy

Averaging. - Of several averaging techniques studied, the following one was considered most satisfactory. The steady-state version of equation (C18) was used in averaging and was applied between the center of a section and its exit. Hence, this method, in effect, replaces the three-section model by a six-section model. Use of the steady-state version of the energy equation allows solution of the section-exit temperature in terms of the section-center temperature. The latter temperature is evaluated by the computer from the dynamic differential energy equation.

Heat-transfer coefficient. - The heat-transfer coefficient used on the water side is the familiar Colburn equation:

$$h_x = \left\{ \frac{0.021}{D^{0.2} A^{0.8}} \left[\left(\frac{C_P}{\mu} \right)^{0.4} k^{0.6} \right]_f \dot{M}^{0.8} \left(\frac{\rho_f}{\rho_b} \right)^{0.8} \right\}_x \tag{D1}$$

This expression is separated into three factors:

$$h_x = \left(G H \dot{M}^{0.8} \right)_x \tag{D2}$$

in which

$$G_x = \left[\frac{0.021}{D^{0.2} A^{0.8}} \left(\frac{\rho_f}{\rho_b} \right)^{0.8} \right]_x \tag{D3}$$

is a constant for each section, and

$$H_x = \left[\left(\frac{C_P}{\mu}\right)^{0.4} k^{0.6}\right]_{x,f} \tag{D4}$$

varies with the waterside film temperature in each section. A plot of the function H_x with film temperature is well approximated by a straight line in the temperature range encountered in the heat exchanger. The linear relation derived is expressed as

$$H_x = 3.739\times10^{-4}\, T_{x,f} - 0.1247 \tag{D5}$$

A plot of $\dot{M}$ against $\dot{M}^{0.8}$ suggested the use of a linear relation between these two variables. In the range applicable to the heat-exchanger water (350 to 1200 lb mass/sec), the relation used was

$$\dot{M}_x^{0.8} = 0.212\, \dot{M}_x + 38 \tag{D6}$$

Within this range the maximum error is less than 5 percent.

Section A. - Application of equation (C18) to section A yields

$$\left(C_P\rho V\right)_{x,A}\frac{dT_{x,A}}{dt} = -\left[\dot{M}C_{P,A}\left(T_{2'} - T_{1'}\right)\right]_x + \left[A_{S,A}G_A H_A \dot{M}^{0.8}\left(T_S - T\right)_A\right]_x \tag{D7}$$

which includes the use of equation (D2). With the assumption

$$T_{x,A} = \frac{1}{2}\left(T_{1'} + T_{2'}\right)_x$$

at steady state, equation (D7) becomes

$$\left[\dot{M}C_{P,A}\left(T_{2'} - T_A\right)\right]_x = \left[\frac{A_{S,A}}{2} G_A H_A \dot{M}^{0.8}\left(T_S - T\right)_A\right]_x$$

This equation is then solved for $T_{x,2'}$, which gives

$$T_{x,2'} = \left[T_A + \left(\frac{GA_S H}{2C_P}\right)_A \left(\frac{\dot{M}^{0.8}}{\dot{M}}\right)\left(T_S - T\right)_A\right]_x \tag{D8}$$

This expression for $T_{x,2'}$ is used in the dynamic version of equation (C18):

$$\left(C_p\rho V\right)_{x,A}\frac{dT_{x,A}}{dt} = -\dot{M}_x C_{P,x,A}\left[T_A + \left(\frac{GA_SH}{2C_P}\right)_A\left(\frac{\dot{M}^{0.8}}{\dot{M}}\right)\left(T_S - T\right)_A - T_{1'}\right]_x$$

$$+\left[\left(GA_SH\right)_A\dot{M}^{0.8}\left(T_S - T\right)_A\right]_x$$

When like terms are combined, this equation becomes

$$\frac{dT_{x,A}}{dt} = \left[\frac{\dot{M}}{(\rho V)_A}\left(T_1 - T_A\right)\right]_x + \left[\left(\frac{GA_SH}{2C_P\rho V}\right)_A\dot{M}^{0.8}\left(T_S - T\right)_A\right]_x \tag{D9}$$

Section B. - The energy equation applied to section B is

$$\left(C_P\rho V\right)_{x,B}\frac{dT_{x,B}}{dt} = -\left[\dot{M}C_{P,B}\left(T_{3'} - T_{2'}\right)\right]_x + \left[\left(A_SGH\right)_B\dot{M}^{0.8}\left(T_S - T\right)_B\right]_x \tag{D10}$$

Solution of this equation at steady state for $T_{x,3'}$ gives

$$T_{x,3'} = \left[T_B + \left(\frac{GA_SH}{2C_P}\right)_B\left(\frac{\dot{M}^{0.8}}{\dot{M}}\right)\left(T_S - T\right)_B\right]_x \tag{D11}$$

This relation and that derived in equation (D8) for $T_{x,2'}$ are substituted into equation (D10):

$$\frac{dT_{x,B}}{dt} = \left[\frac{\dot{M}}{(\rho V)_B}\left(T_A - T_B\right) + \left(\frac{GA_SH}{2C_P\rho V}\right)_A\dot{M}^{0.8}\left(T_S - T\right)_A + \left(\frac{GA_SH}{2C_P\rho V}\right)_B\dot{M}^{0.8}\left(T_S - T\right)_B\right]_x$$

(D12)

Section C. - In section C, the energy equation is

$$C_P \rho V_{x,C} \frac{dT_{x,C}}{dt} = \left[-\dot{M} C_{P,C} \left(T_E - T_{3'}\right)\right]_x + \left[\left(A_S G H\right)_C \dot{M}^{0.8} \left(T_S - T\right)_C\right]_x \qquad \text{(D13)}$$

The heat-exchanger water-exit temperature is evaluated from the steady-state version:

$$T_{x,E} = \left[T_C + \left(\frac{G A_S H}{2 C_P}\right)_C \left(\frac{\dot{M}^{0.8}}{\dot{M}}\right) \left(T_S - T\right)_C\right]_x \qquad \text{(D14)}$$

This equation together with (D11) is used in equation (D13) so that

$$\frac{dT_{x,C}}{dt} = \left[\frac{\dot{M}}{(\rho V)_C} \left(T_B - T_C\right) + \left(\frac{G A_S H}{2 C_P \rho V}\right)_B \dot{M}^{0.8} \left(T_S - T\right)_B + \left(\frac{G A_S H}{2 C_P \rho V}\right)_C \dot{M}^{0.8} \left(T_S - T\right)_C\right]_x \qquad \text{(D15)}$$

Gas Energy

Averaging. - The averaging technique used is the same as that used for the heat-exchanger water.

Heat-transfer coefficient. - The convective heat-transfer coefficient used to express the transfer of heat from wall to hydrogen was obtained from a correlation presented in reference 9:

$$h_X = \left\{\frac{0.021}{D^{0.2} A^{0.8}} \left[\left(\frac{C_P}{\mu}\right)^{0.4} k^{0.6}\right] \left(\frac{T}{T_S}\right)^{0.29 + 0.0019(x/D)} \left(\dot{M}^{0.8}\right)\right\}_X \qquad \text{(D16)}$$

This equation is separated into the following factors:

$$h_X = \left(H b \dot{M}^{0.8}\right)_X \qquad \text{(D17)}$$

where

$$H_X = \left\{ \frac{0.021}{D^{0.2} A^{0.8}} \left[\left(\frac{C_P}{\mu} \right)^{0.4} k^{0.6} \right] \right\}_X \tag{D18}$$

and

$$b_X = \left(\frac{T}{T_S} \right)_X^{0.29+0.0019(x/D)_X} \tag{D19}$$

The length x in the last equation is the distance from the heat-exchanger inlet to the center of a section. The factors H_X and b_X were each assigned a constant value that differed for each section. Several iterations were made by using gas and wall temperatures determined from analog runs before final values of the constants were specified.

The linear relation used for the factor $\dot{M}_X^{0.8}$ was

$$\dot{M}_X^{0.8} = 0.34\,\dot{M}_X + 6 \tag{D20}$$

This approximation is close to an exact value at hydrogen mass-flow rates between 50 and 105 percent of design. At 36.6 percent (the bleed-pump stall limit), it is 4.7 percent too high.

The form of the energy equation used for the heat-exchanger gas is

$$\frac{dT_X}{dt} = \frac{RT_X}{V_X P_X} \left[-\dot{M}\,\Delta T + \frac{hA_S}{C_P} (T_S - T) \right]_X \tag{D21}$$

It includes the use of the perfect-gas equation of state (eq. (C16)). Application of the averaging method described in the heat-exchanger water-energy analysis yields the following equations for the three sections:

Section A:

$$\frac{dT_{X,A}}{dt} = \left(\frac{R}{V_{X,A}} \right) \left(\frac{T}{P} \right)_{X,A} \left[-\dot{M}_X (T_{X,A} - T_{CN,E}) + \left(\frac{A_S Hb}{2C_P} \right)_{X,A} \dot{M}_X^{0.8} (T_S - T)_{X,A} \right] \tag{D22}$$

Section B:

$$\frac{dT_{X,B}}{dt} = \left(\frac{R}{V_{X,B}}\right)\left(\frac{T}{P}\right)_{X,B}\left[-\dot{M}(T_B - T_A) + \left(\frac{A_S Hb}{2C_P}\right)_A \dot{M}^{0.8}(T_S - T)_A + \left(\frac{A_S Hb}{2C_P}\right)_B \dot{M}^{0.8}(T_S - T)_B\right]_X \quad \text{(D23)}$$

Section C:

$$\frac{dT_{X,C}}{dt} = \left(\frac{R}{V_{X,C}}\right)\left(\frac{T}{P}\right)_{X,C}\left[-\dot{M}(T_C - T_B) + \left(\frac{A_S Hb}{2C_P}\right)_B \dot{M}^{0.8}(T_S - T)_B + \left(\frac{A_S Hb}{2C_P}\right)_C \dot{M}^{0.8}(T_S - T)_C\right]_X \quad \text{(D24)}$$

In the course of the derivation of equation (D24), the steady-state form of the energy equation yielded

$$T_{X,E} = \left[T_C + \left(\frac{A_S Hb}{2C_P}\right)_C \left(\frac{\dot{M}^{0.8}}{\dot{M}}\right)(T_S - T)_C\right]_X \quad \text{(D25)}$$

Gas-pressure distribution. - Because only one axial section was used for the heat-exchanger gas momentum equation, a linear pressure variation was assumed to evaluate the pressure at the center of a section. The following relations were used:

$$\Delta P = (P_X - P_{CN})_E \quad \text{(D26)}$$

$$P_{X,A} = P_{CN,E} + \frac{1}{6}\Delta P_X = \frac{5}{6} P_{CN,E} + \frac{1}{6} P_{X,E} \quad \text{(D27)}$$

$$P_{X,B} = P_{CN,E} + \frac{1}{2}\Delta P_X = \frac{1}{2}(P_{CN} + P_X)_E \quad \text{(D28)}$$

$$P_{X,C} = P_{CN,E} + \frac{5}{6}\Delta P_X = \left(\frac{1}{6} P_{CN} + P_X\right)_E \quad \text{(D29)}$$

Gas Momentum

For the one axial section employed to simulate the momentum equation applied to the heat-exchanger gas, the form of equation (C4) used was

$$\frac{d\dot{M}_X}{dt} = -g\left(\frac{A_{X,S}}{\Delta x}\right)_{He} \Delta P_X + \left(\frac{\dot{M}^2}{\rho V}\right)_X \left[\left(\frac{\Delta\rho}{\rho}\right)_X - \left(\frac{2f\ \Delta x}{D}\right)_{He}\right] \tag{D30}$$

Calculation of the following parameters is necessary for insertion into equation (D30):

$$\Delta\rho_X = \left(\rho_X - \rho_{CN}\right)_E \tag{D31}$$

$$\rho_X = \frac{1}{2}\left(\rho_{CN} + \rho_X\right)_E \tag{D32}$$

$$\frac{d\rho_{X,E}}{dt} = \frac{1}{V_{X-T}}\left(\dot{M}_X - \dot{M}_{TT} - \dot{M}_5\right) \tag{D33}$$

$$\Delta P_X = \left(P_X - P_{CN}\right)_E \tag{D34}$$

$$P_{X,E} = \rho_{X,E} R T_{X,E} \tag{D35}$$

$$f = \frac{0.84\ Z}{\left(\ln Re_{X,f} - 1.11\right)^{2.22}} \tag{D36}$$

In equation (D36), the factor Z represents the friction entrance and exit effects due to contraction as the hydrogen gas enters the heat-exchanger tubes and expansion as it emerges. The remainder of the expression in equation (D36) was derived from a plot of the Karman-Nikuradse approximation for friction in fluid flow.

Tube

Averaging. - Within the tube material, the radial temperature variation was assumed to be linear. With T_W representing the temperature at the center of the section on the water side and T_H the center temperature on the cold hydrogen side, the surface temperatures are expressed as follows:

Waterside surface:

$$T_{x,S} = 1.5\,T_W - 0.5\,T_H \tag{D37}$$

Gasside surface:

$$T_{X,S} = 1.5\,T_H - 0.5\,T_W \tag{D38}$$

These equations were used in the heat-exchanger water analysis (eqs. (D9), (D12), (D14), and (D15)) and gas analysis (eqs. (D22) to (D25)).

Energy equation. - A heat balance applied to the waterside section yields

$$\left(\rho V C_P\right)_{He} \frac{dT_W}{dt} = h_x A_{x,S}\left(T - T_S\right)_x - \left(\frac{kA}{y}\right)_{He}\left(T_W - T_H\right) \tag{D39}$$

and to the gas side is

$$\left(\rho V C_P\right)_{He} \frac{dT_H}{dt} = -h_X A_{X,S}\left(T_S - T\right)_X + \left(\frac{kA}{y}\right)_{He}\left(T_W - T_H\right) \tag{D40}$$

Application of these two equations to axial section A gives

$$\frac{dT_{W,A}}{dt} = \frac{\left(GA_S H\right)_{x,A}}{\left(\rho V C_P\right)_{He}} \dot{M}_X^{0.8}\left(T_x + 0.5\,T_H - 1.5\,T_W\right)_A - \left(\frac{kA}{\rho V C_P y}\right)_{He}\left(T_W - T_H\right)_A \tag{D41}$$

and

$$\frac{dT_{H,A}}{dt} = -\frac{\left(A_S Hb\right)_{X,A}}{\left(\rho V C_P\right)_{He}} \dot{M}_X^{0.8}\left(1.5\,T_H - 0.5\,T_W - T_X\right)_A + \left(\frac{kA}{\rho V C_P y}\right)_{He}\left(T_W - T_H\right)_A \tag{D42}$$

The equations for axial sections B and C are identical to the preceding two equations except that subscript A is replaced by B and C, respectively.

CORE

Gas Energy

Heat-transfer coefficient. - The form of equation (D16) was used again to express the convective heat-transfer coefficient between the hydrogen gas and fuel surface. In this instance, it was separated into two factors:

$$h_c = \left(H\dot{M}^{0.8}\right)_c \tag{D43}$$

The factor

$$H_c = \left\{ \frac{0.021}{D^{0.2} A^{0.8}} \left[\left(\frac{C_P}{\mu} \right)^{0.4} k^{0.6} \right]_b \left(\frac{T_b}{T_{Wall}} \right)^{0.302} \right\}_c \tag{D44}$$

is a constant that has a different value for each of the three sections. Several iterations were made to establish the final values used. Equation (D20) was used again to evaluate $\dot{M}_c^{0.8}$ and has the same range of accuracy.

Section A. - The basic form of the energy equation used is similar to that applied to the heat-exchanger gas.

$$\frac{dT_{c,A}}{dt} = \left(\frac{R}{V_{c,A}} \right) \left(\frac{T}{P} \right)_{c,A} \left[-\dot{M}_c \left(T_{2'} - T_I \right)_c + \left(\frac{A_F, S^{H_c}}{C_{P,c}} \right)_A \dot{M}_c^{0.8} \left(T_F - T_c \right)_A \right] \tag{D45}$$

When $dT_{c,A}/dt$ is set equal to zero in equation (D45), insertion of the resultant expression for $T_{c,2'}$ into this equation yields

$$\frac{dT_{c,A}}{dt} = \left(\frac{R}{V_{c,A}} \right) \left(\frac{T}{P} \right)_{c,A} \left[\dot{M}_c \left(T_I - T_A \right)_c + \left(\frac{A_F, S^{H_c}}{2C_{P,c}} \right)_A \dot{M}_c^{0.8} \left(T_F - T_c \right)_A \right] \tag{D46}$$

The value of $T_{c,I}$ is determined by

$$T_{c,I} = \left(\frac{T_{c,I}}{T_{X,E}} \right)_{ref} T_{X,E} \tag{D47}$$

The approximation in equation (D47) is good because the small temperature drop across the topping turbine subtracts from the small hydrogen gas temperature rise in the shield. The factor $(T_{c,I}/T_{X,E})_{ref}$, which is slightly greater than 1, was assigned a different reference value for each set of bleed-valves settings.

Section B. - After the steady-state energy equation is solved for $T_{c,3'}$, the dynamic version becomes

$$\frac{dT_{c,B}}{dt} = \left(\frac{R}{V_{c,B}}\right)\left(\frac{T}{P}\right)_{c,B}\left[\dot{M}_c\left(T_A - T_B\right)_c + \left(\frac{A_{F,S}H_c}{2C_{P,c}}\right)_A \dot{M}_c^{0.8}\left(T_F - T_c\right)_A + \left(\frac{A_{F,S}H_c}{2C_{P,c}}\right)_B \dot{M}_c^{0.8}\left(T_F - T_c\right)_B\right] \tag{D48}$$

Section C. - The corresponding equation for section C is

$$\frac{dT_{c,C}}{dt} = \left(\frac{R}{V_{c,C}}\right)\left(\frac{T}{P}\right)_{c,C}\left[\dot{M}_c\left(T_B - T_C\right)_c + \left(\frac{A_{F,S}H_c}{2C_{P,c}}\right)_B \dot{M}_c^{0.8}\left(T_F - T_c\right)_B + \left(\frac{A_{F,S}H_c}{2C_{P,c}}\right)_C \dot{M}_c^{0.8}\left(T_F - T_c\right)_C\right] \tag{D49}$$

The core-gas exit temperature $T_{c,E}$, determined in deriving equation (D49), is

$$T_{c,E} = T_{c,C} + \left(\frac{A_{F,S}H_c}{2C_{P,c}}\right)\left(\frac{\dot{M}^{0.8}}{\dot{M}}\right)_c \left(T_F - T_c\right)_C \tag{D50}$$

Gas-pressure distribution. - The core-gas-pressure distribution was assumed to be linear because only one axial section was used in the mass-flow rate calculation:

$$\Delta P_c = P_{c,E} - P_{c,I} \tag{D51}$$

$$P_{c,A} = P_{c,I} + \frac{1}{8}\Delta P_c \tag{D52}$$

$$P_{c,B} = P_{c,I} + \frac{3}{8}\Delta P_c \tag{D53}$$

$$P_{c,C} = P_{c,I} + \frac{3}{4}\Delta P_c \tag{D54}$$

Gas Momentum

Application of the momentum equation (C4) to the one-axial section results in

$$\frac{d\dot{M}_c}{dt} = \left\{ -\left(\frac{gA}{\Delta x}\right)\Delta P + \left(\frac{\dot{M}^2}{\rho V}\right)\left[\frac{\Delta\rho}{\rho} - \left(\frac{2f\ \Delta x}{D}\right) - K\ \Delta x\right]\right\}_c \tag{D55}$$

The last term represents the entrance and exit losses of the individual axial stages of the fuel elements. The following parameters were evaluated in solving equation (D55):

$$\Delta\rho_c = \left(\rho_E - \rho_I\right)_c \tag{D56}$$

$$\frac{d\rho_{c,E}}{dt} = \frac{1}{V_{c-N}}\left(\dot{M}_c - \dot{M}_N\right) \tag{D57}$$

Preliminary digital calculations of a multisection model of the core gas revealed that the axial variation of $1/\rho_c$ is nearly linear. The relation used is

$$\frac{1}{\rho_c} = \left[\frac{2}{3}\left(\frac{1}{\rho_B}\right) + \frac{1}{3}\left(\frac{1}{\rho_C}\right)\right]_c \tag{D58}$$

Since two points determine a straight line, $1/\rho_{c,A}$ could have been used in this expression instead of $1/\rho_{c,B}$ or $1/\rho_{c,C}$ with an appropriate adjustment in the constants. The core-gas density factors were evaluated by

$$\frac{1}{\rho_{c,B}} = R\left(\frac{T}{P}\right)_{c,B} \tag{D59}$$

and

$$\frac{1}{\rho_{c,C}} = R\left(\frac{T}{P}\right)_{c,C} \tag{D60}$$

$$f_c = \frac{0.84\ Z}{(\ln Re_c - 1.11)^{2.22}} \tag{D61}$$

Core-gas exit pressure was calculated from

$$P_{c,E} = \rho_{c,E} R T_{c,E} \tag{D62}$$

FUEL

A heat balance in the cylindrical model of the fuel elements included heat generation. The three axial sections used corresponded to those in the core-gas analysis. The heat-generation rates in each section were based on the axial fuel distribution rates:

Section A:

$$\frac{dT_{F,A}}{dt} = -\left(\frac{H_c}{\rho_F C_{P,F} y_F}\right)_A \dot{M}_c^{0.8}\left(T_F - T_c\right)_A + \left(\frac{\dot{Q}}{\rho V C_P}\right)_{F,A} \tag{D63}$$

$$\dot{Q}_{F,A} = 0.278\ \dot{Q}_{TOT} \tag{D64}$$

Section B:

$$\frac{dT_{F,B}}{dt} = -\left(\frac{H_c}{\rho_F C_{P,F} y_F}\right)_B \dot{M}_c^{0.8}\left(T_F - T_c\right)_B + \left(\frac{\dot{Q}}{\rho V C_P}\right)_{F,B} \tag{D65}$$

$$\dot{Q}_{F,B} = 0.325\ \dot{Q}_{TOT} \tag{D66}$$

Section C:

$$\frac{dT_{F,C}}{dt} = -\left(\frac{H_c}{\rho_F C_{P,F} y_F}\right)_C \dot{M}_c^{0.8}\left(T_F - T_c\right)_C + \left(\frac{\dot{Q}}{\rho V C_P}\right)_{F,C} \tag{D67}$$

$$\dot{Q}_{F,C} = 0.365\ \dot{Q}_{TOT} \tag{D68}$$

MODERATOR WATER

The moderator water flows through the core in two annular passages separated by an aluminum flow divider. To distinguish between the two moderator waters, the volumes inside and outside the flow divider are referred to herein as "inside" and "outside" water.

Heat-Transfer Coefficient

The convective heat-transfer coefficient used was the same as that used for the heat-exchanger water:

$$h_w = \left\{ \frac{0.021}{D^{0.2} A^{0.8}} \left[\left(\frac{C_P}{\mu} \right)^{0.4} k^{0.6} \right]_f \dot{M}^{0.8} \left(\frac{\rho_f}{\rho_b} \right)^{0.8} \right\}_w \tag{D69}$$

$$h_w = \left(H \dot{M}^{0.8} \right)_w \tag{D70}$$

The factor

$$H_w = \left\{ \frac{0.021}{D^{0.2} A^{0.8}} \left[\left(\frac{C_P}{\mu} \right)^{0.4} k^{0.6} \right]_f \left(\frac{\rho_f}{\rho_b} \right)^{0.8} \right\}_w \tag{D71}$$

was assigned a constant value, determined after several iterations, for each passage.

For the range of flow rate of both the inside and outside water, the following linear expressions for $\dot{M}^{0.8}$ were used:

$$\left.\begin{aligned} \dot{M}_{w,i}^{0.8} &= 0.235\, \dot{M}_{w,i} + 25 \\ \dot{M}_{w,o}^{0.8} &= 0.235\, \dot{M}_{w,o} + 25 \end{aligned}\right\} \tag{D72}$$

This relation is applicable in the flow rate range between 200 and 800 pounds mass per second, within which the maximum error is 3.6 percent. Throughout the analysis, the inside and outside water mass-flow rates were assumed to be constant fractions of the total, the constants being evaluated at the 100-percent design point:

$$\dot{M}_{w,i} = 0.423\ \dot{M}_w \tag{D73}$$

$$\dot{M}_{w,o} = 0.487\ \dot{M}_w \tag{D74}$$

The two heat-transfer coefficients on each of the inside water boundaries were assumed equal.

$$h_{D,i} = h_{PT,o} = h_i \tag{D75}$$

Energy Equation for Inside Water

Heat enters the inside water by convection from the pressure-tube and flow-divider surfaces and by internal generation:

$$\frac{dT_{w,i}}{dt} = -\left(\frac{\dot{M}\,\Delta T}{\rho V}\right)_{w,i} + \frac{A_{PT,S}H_{w,i}}{(\rho V C_P)_{w,i}}\,\dot{M}_{w,i}^{0.8}(T_{PT} - T_{w,i}) + \left[\frac{A_{D,S}H_w}{(\rho V C_P)_w}\right]_i \dot{M}_{w,i}^{0.8}(T_D - T_{w,i}) + \left(\frac{\dot{Q}}{\rho V C_P}\right)_{w,i} \tag{D76}$$

$$\Delta T_{w,i} = 2(T_{w,i} - T_{x,E}) \tag{D77}$$

$$\dot{Q}_{w,i} = 0.00598\ \dot{Q}_{TOT} \tag{D78}$$

Energy Equation for Outside Water

Only one surface, the flow-divider outer surface, supplies convected heat to the outside water. Therefore,

$$\frac{dT_{w,o}}{dt} = -\left(\frac{\dot{M}\,\Delta T}{\rho V}\right)_{w,o} + \left[\frac{A_{D,S}H_w}{(\rho V C_P)_w}\right]_o \dot{M}_{w,o}^{0.8}(T_D - T_{w,o}) + \left(\frac{\dot{Q}}{\rho V C_P}\right)_{w,o} \tag{D79}$$

$$\Delta T_{w,o} = 2(T_{w,o} - T_{x,E}) \tag{D80}$$

$$\dot{Q}_{w,o} = 0.01600\ \dot{Q}_{TOT} \tag{D81}$$

PRESSURE TUBE

Heat enters the pressure tube by conduction through the stagnant hydrogen layer into its inner surface and by heat generation within its material. Heat leaves the pressure tube outer surface by convection into the inside water. A heat balance applied to the pressure tube gives

$$\frac{dT_{PT}}{dt} = \frac{A_{PT,S}{}^{H_{w,i}}}{(\rho VC_P)_{PT}} \dot{M}_{w,i}^{0.8}(T_{w,i} - T_{PT}) + \frac{\dot{Q}_{SH} + \dot{Q}_{PT}}{(\rho VC_P)_{PT}} \tag{D82}$$

The heat loss from the core gas conducted through the stagnant hydrogen layer $\dot{Q}_{SH}$ is assumed to be a linear function of the total heat rate produced. It also includes the effect of thermal radiation. This heat loss was evaluated at 20 and 100 percent to determine the function:

$$\dot{Q}_{SH} = 0.00255\ \dot{Q}_{TOT} + 2879 \tag{D83}$$

The heat generated within the aluminum material of the pressure tube is proportional to the total heat rate:

$$\dot{Q}_{PT} = 0.00218\ \dot{Q}_{TOT} \tag{D84}$$

FLOW DIVIDER

Heat is generated within the material and leaves through its inner and outer surfaces by convection into the inside and outside water, respectively. The heat balance is

$$\frac{dT_D}{dt} = \frac{(A_{D,S}{}^{H_w})_i}{(\rho VC_P)_D} \dot{M}_{w,i}^{0.8}(T_{w,i} - T_D) + \frac{(A_{D,S}{}^{H_w})_o}{(\rho VC_P)_D} \dot{M}_{w,o}^{0.8}(T_{w,o} - T_D) + \left(\frac{\dot{Q}}{\rho VC_P}\right)_D \tag{D85}$$

$$\dot{Q}_D = 0.00132\ \dot{Q}_{TOT} \tag{D86}$$

SIDE REFLECTOR

Heat-Transfer Coefficient

The convective heat-transfer coefficient used is defined by equations (D69), (D70), and (D71) with the subscript R preceding w. The linear relation used for $\dot{M}^{0.8}_{R,w}$ is

$$\dot{M}^{0.8}_{R,w} = 0.34\,\dot{M}_{R,w} + 6 \tag{D87}$$

where

$$\dot{M}_{R,w} = 0.090\,\dot{M}_{w} \tag{D88}$$

The linear expression in equation (D87) is applicable in the mass-flow rate range of 35 to 120 pounds mass per second, within which the maximum deviation is 3.5 percent.

Water Energy

Heat enters the reflector water by convection from the reflector wall and by generation within the water. The energy equation is

$$\frac{dT_{R,w}}{dt} = \left[-\left(\frac{\dot{M}\,\Delta T}{\rho V}\right)_w + \frac{A_S H_w}{(\rho V C_P)_w}\,\dot{M}^{0.8}_{w}(T - T_w) + \left(\frac{\dot{Q}}{\rho V C_P}\right)_w \right]_R \tag{D89}$$

$$\Delta T_{R,w} = 2(T_{R,w} - T_{x,E}) \tag{D90}$$

$$\dot{Q}_{R,w} = 4.57\times10^{-4}\,\dot{Q}_{TOT} \tag{D91}$$

Reflector Material

Heat is generated within the reflector material and is convected from its wall into the reflector water. The heat balance is

$$\frac{dT_R}{dt} = \left[\frac{A_S H_w}{\rho V C_P}\,\dot{M}^{0.8}(T_w - T) + \left(\frac{\dot{Q}}{\rho V C_P}\right) \right]_R \tag{D92}$$

$$\dot{Q}_R = 0.00340\,\dot{Q}_{TOT} \tag{D93}$$

REFLECTOR- AND CORE-WATER EXIT MIXING

The three water streams of the reactor mix in an outlet plenum. For a heat balance in the plenum,

$$\frac{dT_{mmw}}{dt} = \frac{1}{(\rho V)_{mmw}} \left(\dot{M}_{w,i} T_{w,i,E} + \dot{M}_{w,o} T_{w,o,E} + \dot{M}_{R,w} T_{R,w,E} - \dot{M}_x T_{mmw} + \frac{\dot{Q}_x}{C_{P,mmw}} \right) \tag{D94}$$

The term $\dot{Q}_x$ is the heat generated in the heat-exchanger water; it is lumped with the water-plenum mixing for simplicity. This parameter is evaluated as

$$\dot{Q}_x = 4.24 \times 10^{-4} \dot{Q}_{TOT} \tag{D95}$$

WATER-FLOW LOOP

Application of the momentum equation to the water-flow loop yields

$$\frac{d\dot{M}_w}{dt} = \frac{gA^2}{V_w} (\Delta P_{WP} - \Delta P_{w,fr}) \tag{D96}$$

The friction pressure drop in the water loop is assumed to be

$$\Delta P_{w,fr} = 0.02037 \dot{M}_w^2 \tag{D97}$$

BLEED SYSTEM

Gas Energy

The heat-transfer coefficient of reference 9 was also used in the bleed system analysis. It is expressed as

$$h_{BG} = \frac{0.021}{(D^{0.2} A^{0.8})_{BG}} \left[\left(\frac{C_P}{\mu} \right)^{0.4} k^{0.6} \right]_{BG} \left(\frac{T_{BG}}{T_{BF}} \right)^{0.29+0.0019(x/D)_{BG}} \left(\dot{M}_{BG}^{0.8} \right) \tag{D98}$$

and

$$h_{BG} = \left(H\dot{M}^{0.8}\right)_{BG} \tag{D99}$$

In the bleed system, H_{BG}, which is a function of bleed fuel geometry, gas properties, and bleed-gas temperature, was assumed constant. Several iterations preceded the final determination of the constant. A plot of $\dot{M}_{BG}^{0.8}$ against $\dot{M}_{BG}$ in the range between 0.8 and 3.3 pounds mass per second, as used in the bleed system, is essentially linear. The form used is

$$\dot{M}_{BG}^{0.8} = 0.0235\ \dot{M}_{BG} + 0.3133 \tag{D100}$$

The maximum error within this range is 5 percent.

Equation (C18), when applied to the one-section model of the bleed system, yields

$$\frac{dT_{BG}}{dt} = R\left(\frac{T}{PV}\right)_{BG}\left[-(\dot{M}\ \Delta T)_{BG} + \left(\frac{A_{B,S}H_{BG}}{C_{P,BG}}\right)\dot{M}_{BG}^{0.8}(T_{BF} - T_{BG})\right] \tag{D101}$$

In this equation

$$\Delta T_{BG} = T_{B,E} - T_{c,I} \tag{D102}$$

and

$$P_{BG} = \frac{1}{2}\left(P_{c,I} + P_{B,E}\right) \tag{D103}$$

Gas Momentum

The momentum equation (C4) applied to the bleed system is

$$\frac{d\dot{M}_{BG}}{dt} = -g\left(\frac{A}{\Delta x}\ \Delta P\right)_{BG} + \left\{\left(\frac{\dot{M}^2}{\rho V}\right)\left[\left(\frac{\Delta\rho}{\rho}\right) - \left(\frac{2f\ \Delta x}{D}\right) - K\ \Delta x\right]\right\}_{BG} \tag{D104}$$

The following relations are used in this expression:

$$\Delta P_{BG} = P_{B,E} - P_{c,I} \tag{D105}$$

$$\Delta \rho_{BG} = \rho_1 - \rho_{c,I} \tag{D106}$$

$$P_{B,E} = P_1 + 0.1097\, \dot{M}_{BG}^2 \tag{D107}$$

$$\rho_{BG} = \frac{1}{2}(\rho_1 + \rho_{c,I}) \tag{D108}$$

$$f_{BG} = \frac{0.84\, Z}{\ln\left(Re_{BG,f} - 1.11\right)^{2.22}} \tag{D109}$$

Fuel

A heat balance applied to the solid fuel materials yields

$$\frac{dT_{BF}}{dt} = -\left[\frac{H_{BG}}{\left(\rho C_P \frac{\Delta y}{2}\right)_{BF}}\right] \dot{M}_{BG}^{0.8}(T_{BF} - T_{BG}) + \left(\frac{\dot{Q}}{\rho V C_p}\right)_{BF} \tag{D110}$$

$$\dot{Q}_{BF} = 0.0101\, \dot{Q}_{TOT} \tag{D111}$$

The approximation of equation (D111) was used to eliminate the necessity of simulating the kinetics equations in the bleed system.

NOZZLES

Nozzle Coolant

Energy equation. - The following equation was applied to calculate the gas temperature at the center of the nozzle-coolant section.

$$\frac{dT_{CN}}{dt} = \left\{\left(\frac{1}{\rho V}\right)\left[-\dot{M}(T_E - T_I) + \left(\frac{hA_S}{C_P}\right)(T_{Wall} - T)\right]\right\}_{CN} \tag{D112}$$

In this equation, the convective heat-transfer coefficient is expressed as

$$h_{CN} = 0.0182\ \dot{M}_{CN}^{0.8} \tag{D113}$$

where

$$\dot{M}_{CN}^{0.8} = 0.34\ \dot{M}_{CN} + 6 \tag{D114}$$

as used in the heat-exchanger and core-gas simulations, and

$$\frac{d\rho_{CN,E}}{dt} = \left(\frac{1}{V_{CN-X}}\right)(\dot{M}_{CN} - \dot{M}_X) \tag{D115}$$

$$\rho_{CN} = \frac{1}{2}\left(\rho_I + \rho_E\right)_{CN} \tag{D116}$$

$$T_{CNW} = 0.2108\ T_{c,E} \tag{D117}$$

$$T_{CN,E} = 2T_{CN} - T_{CN,I} \tag{D118}$$

The nozzle-coolant inlet temperature $T_{CN,I}$ was assigned a different constant value for each set of bleed-valves settings.

Momentum equation. - Application of equation (C4) yields

$$\frac{d\dot{M}_{CN}}{dt} = -g\left(\frac{A}{\Delta x}\,\Delta P\right)_{CN} - 3.486\ \dot{M}_{CN}^2 \tag{D119}$$

in which

$$-\Delta P_{CN} = P_o + \Delta P_{BP} + \Delta P_{TP} - P_{CN,E} \tag{D120}$$

and

$$P_{CN,E} = \rho_{CN,E} R T_{CN,E} \tag{D121}$$

Nozzle-Gas Flow

Both the thrust and bleed nozzles are assumed to be choked throughout the analysis. For isentropic flow the mass-flow rate is

$$\dot{M} = A \frac{P}{\sqrt{T}} \sqrt{\frac{\gamma g}{R} \left(\frac{2}{\gamma + 1} \right)^{\gamma + 1/\gamma - 1}} \tag{D122}$$

With the use of the perfect gas relation, this equation becomes for the thrust nozzle

$$\dot{M}_N = 107.7 \, A_N \rho_{c,E} \sqrt{T_{c,E}} \tag{D123}$$

and for the bleed nozzle

$$\dot{M}_{BN} = 107.7 \, A_{BN} \rho_{4,E} \sqrt{T_{4,E}} \tag{D124}$$

PUMPS

A conventional pump-performance map relating pressure rise and flow rate can be compressed into a single curve when plotted as $\Delta P/N^2$ against $\dot{M}/N$. Likewise, one curve relates L/N^2 with $\dot{M}/N$. For the three pumps, the six variations on such plots were set on variable diode function generators, as indicated in the following equations:

Bleed pump:

$$\left(\frac{\Delta P}{N^2} \right)_{BP} = G'_{BP} \left(\frac{\dot{M}_{CN}}{N_{BP}} \right) \tag{D125}$$

$$\left(\frac{L}{N^2} \right)_{BP} = g'_{BP} \left(\frac{\dot{M}_{CN}}{N_{BP}} \right) \tag{D126}$$

Topping-driven pump:

$$\left(\frac{\Delta P}{N^2}\right)_{TP} = G'_{TP}\left(\frac{\dot{M}_{CN}}{N_{TP}}\right) \tag{D127}$$

$$\left(\frac{L}{N^2}\right)_{TP} = g'_{TP}\left(\frac{\dot{M}_{CN}}{N_{TP}}\right) \tag{D128}$$

Water pump:

$$\left(\frac{\Delta P}{N^2}\right)_{WP} = G'_{WP}\left(\frac{\dot{M}_x}{N_{WP}}\right) \tag{D129}$$

$$\left(\frac{L}{N^2}\right)_{WP} = g'_{WP}\left(\frac{\dot{M}_x}{N_{WP}}\right) \tag{D130}$$

TURBINES

Water-Pump Turbine

Torque. - The relation between $L_{WT}/\dot{M}_{WT}\sqrt{T_1}$ and $N_{WT}/\sqrt{T_1}$ is linear for a constant pressure ratio. In addition, a plot of $L_{WT}/\dot{M}_{WT}\sqrt{T_1}$ against the pressure-ratio function

$$\sqrt{1 - \left(\frac{P_E}{P_I}\right)^{(\gamma-1)/\gamma}}$$

is linear for the zero-speed condition. When these two linear relations are combined, the following equations result:

$$\left(\frac{L_{WT}}{\dot{M}_{WT}\sqrt{T_1}}\right) = 16.46\sqrt{1 - \left(\frac{P_2}{P_1}\right)^{(\gamma-1)/\gamma}_E} - 0.0045\left(\frac{N_{WT}}{\sqrt{T_1}}\right)$$

or

$$L_{WT} = \dot{M}_{WT}\left(16.46\sqrt{T_1}\, f'_{WT} - 0.0045\, N_{WT}\right) \tag{D131}$$

In equation (D131), the function is provided by a variable diode function generator

$$f'_{WT} = \sqrt{1 - \left(\frac{P_E}{P_I}\right)^{(\gamma-1)/\gamma}} \tag{D132}$$

Mass-flow rate. - The function

$$F'_{WT} = \frac{\dot{M}_{WT}\sqrt{T_1}}{P_{1,E}} \tag{D133}$$

was set on a variable diode function generator. Water-pump turbine mass-flow rate was determined from

$$\dot{M}_{WT} = \left(\frac{P_{1,E}}{\sqrt{T_1}}\right) F'_{WT} \tag{D134}$$

Speed. - The turbine and pump torques are used in calculating rotational speed:

$$\frac{dN_{WT}}{dt} = \left(\frac{30}{\pi I_{WTP}}\right)(L_{WT} - L_{WP}) \tag{D135}$$

Hydrogen Bleed-Pump Turbine

Torque. - The torque-parameter plot of the hydrogen bleed-pump turbine also has linear characteristics, in the manner discussed in connection with the water-pump turbine. The linear equation obtained is

$$\left(\frac{L_{BT}}{\dot{M}_{BT}\sqrt{T_{c,E}}}\right) = 22.1\sqrt{1 - \left(\frac{P_4}{P_3}\right)^{(\gamma-1)/\gamma}_E} - 0.0082\left(\frac{N_{BT}}{\sqrt{T_{3,E}}}\right) \tag{D136}$$

Again, a variable diode function generator was set with the same pressure ratio function

$$f'_{BT} = f'_{WT} = \sqrt{1 - \left(\frac{P_E}{P_I}\right)^{(\gamma-1)/\gamma}} \qquad \text{(D137).}$$

as that used for the water-pump turbine. Accordingly, the form of the torque equation used is

$$L_{BT} = \dot{M}_{BT}\left(22.1\sqrt{T_{3,E}}\, f'_{BT} - 0.0082\, N_{BT}\right) \qquad \text{(D138)}$$

The value of $T_{3,E}$ used was approximated by

$$T_{3,E} = \left(\frac{T_{3,E}}{T_1}\right)_{ref} T_1 \qquad \text{(D139)}$$

in which $\left(T_{3,E}/T_1\right)_{ref}$ was assigned the design value when the bleed valves were set at the 100 percent positions. The values at the other two reference points were used for the 60 and 36.6 percent settings. The temperature drop across the water-pump turbine is less than 4 percent; thus, the assumption in equation (D139) is very good. The pressure $P_{3,E}$, used in equation (D136), is determined from equation (D170). The pressure $P_{4,E}$ is calculated by

$$P_{4,E} = \rho_{4,E} R T_{4,E} \qquad \text{(D140)}$$

in which

$$T_{4,E} = \left(\frac{T_{4,E}}{T_1}\right)_{ref} T_1 \qquad \text{(D141)}$$

and

$$\frac{d\rho_{4,E}}{dt} = \frac{1}{V_{4\text{-}N}}\left(\dot{M}_{BT} + \dot{M}_4 - \dot{M}_{BN}\right) \qquad \text{(D142)}$$

The assumption of constant temperature ratio across the bleed-pump turbine (eq. (D141)) is not as valid as that used in the water-pump turbine because the former turbine has a greater work output. At the 100 percent design point, the temperature at the bleed-pump

turbine inlet drops by 14 percent. Smaller percentage drops occur at lower power levels. The 14 percent is not an error, of course. Furthermore, a different reference value is used for $\left(T_{4,E}/T_1\right)_{ref}$ at each of the three bleed-valves settings.

Mass-flow rate. - Because the bleed-pump turbine is choked at design conditions, the following relation was used:

$$\dot{M}_{BT} = 0.00386 \frac{P_{3,E}}{\sqrt{T_{3,E}}} \tag{D143}$$

With the use of the equation of state (eq. (C16)), this equation becomes

$$\dot{M}_{BT} = 2.96\, \rho_{3,E} \sqrt{T_{3,E}} \tag{D144}$$

This approximation reduces the amount of analog equipment required. A 2-percent error occurs if the turbine pressure ratio drops from 5.5 to 4.0. An error of this magnitude is within the accuracy of analog work.

Speed. - The dynamic equation for turbine (and pump) speed is similar to that used for the water-pump turbine:

$$\frac{dN_{BT}}{dt} = \frac{30}{\pi I_{BTP}} \left(L_{BT} - L_{BP}\right) \tag{D145}$$

Topping Turbine

Torque. - The following linear relation also proved applicable to the topping turbine torque representation:

$$\frac{L_{TT}}{\dot{M}_{TT}\sqrt{T_{X,E}}} = 8.8 \sqrt{1 - \left(\frac{P_{TT,E}}{P_{TT,I}}\right)^{(\gamma-1)/\gamma}} - 9.36 \times 10^{-4} \frac{N_{TT}}{\sqrt{T_{X,E}}} \tag{D146}$$

As for the other turbines, the pressure-ratio function was set on a variable diode function generator

$$f'_{TT} = f'_{BT} = f'_{WT} = \sqrt{1 - \left(\frac{P_E}{P_I}\right)^{(\gamma-1)/\gamma}} \tag{D147}$$

Thus, the topping-turbine torque was simulated by

$$L_{TT} = \dot{M}_{TT}\left(8.8\sqrt{T_{X,E}}\, f'_{TT} - 9.36\times10^{-4}\, N_{TT}\right) \tag{D148}$$

In this equation it is assumed that

$$T_{TT,I} = T_{X,E} \tag{D149}$$

Mass-flow rate. - A variable diode function generator was set with the function

$$F'_{TT} = \frac{\dot{M}_{TT}\sqrt{T_{X,E}}}{P_{TT,I}}$$

The mass-flow rate was calculated from

$$\dot{M}_{TT} = \frac{P_{TT,I}}{\sqrt{T_{X,E}}}\, F'_{TT} \tag{D150}$$

Speed. - The same rotational speed equation is used

$$\frac{dN_{TT}}{dt} = \left(\frac{30}{\pi I_{TTP}}\right)(L_{TT} - L_{TP}) \tag{D151}$$

Exit pressure. - Topping-turbine exit pressure was calculated by adding a friction pressure change between core inlet and turbine exit. This pressure drop was assumed to be proportional to the square of the total hydrogen mass-flow rate.

$$P_{TT,E} = P_{c,I} + 1.04\left(\dot{M}_{TT} + \dot{M}_5\right)^2 \tag{D152}$$

A different value of the constant in this equation was used at each of the three bleed-valves settings.

The core-gas inlet pressure was calculated by using the following relations:

$$\frac{d\rho_{c,I}}{dt} = \frac{1}{V_{T-c}}\left(\dot{M}_{TT} + \dot{M}_5 - \dot{M}_c - \dot{M}_{BG}\right) \tag{D153}$$

$$P_{c,I} = \rho_{c,I} R T_{c,I} \tag{D154}$$

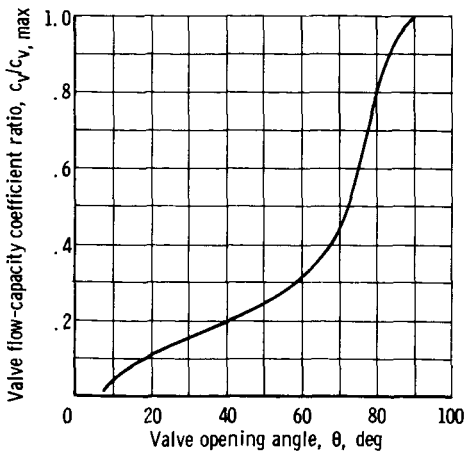

Figure 12. - Typical experimental butterfly-valve characteristics.

VALVES

The range of pressures and temperatures and the absence of a positive shutoff requirement permitted the use of butterfly-type valves. The need of selecting a valve size was eliminated by employing a relation between valve flow-capacity coefficient ratio $c_v/c_{v,max}$ and stem position. A plot of the characteristics of a typical experimental butterfly valve is presented in figure 12.

The following equations were used to calculate the mass-flow rate passed by a valve:

For nonchoked flow:

$$\dot{M} = 0.008\, c_v \sqrt{\frac{P_E}{T_I}(P_I - P_E)} \tag{D155}$$

For choked flow:

$$\dot{M} = 0.004\, c_v \frac{P_I}{\sqrt{T_I}} \tag{D156}$$

In the application of these equations to the computer, a relay was used with the simulation of the two water-pump turbine valves and the bleed-pump-turbine throttle valve to provide for choking or nonchoking flow. Valve pressure ratio was used as a basis of the relay operation. In the following explicit mass-flow rate equations for these valves, only the nonchoked relation is given, it being understood that the relay makes the appropriate selection. Because the bleed-turbine bypass valve is choked at the three reference points, it is assumed to be choked throughout the simulation. Also, the topping-turbine bypass valve is assumed to be nonchoked throughout because it is not choked at the design point.

Water-Pump-Turbine Bypass Valve

This valve is designated herein as valve 1. The mass-flow rate it passes is

$$\dot{M}_1 = 0.008 \left[c_v \frac{P}{\sqrt{T}} \sqrt{\frac{P_E}{P} - \left(\frac{P_E}{P}\right)^2} \right]_1 \tag{D157}$$

The following variables are calculated for use in this equation:

$$\frac{d\rho_1}{dt} = \frac{1}{V_{B-1}} (\dot{M}_{BG} - \dot{M}_1 - \dot{M}_2) \tag{D158}$$

$$T_1 = \left(\frac{T_1}{T_{BG}}\right)_{ref} T_{BG} \tag{D159}$$

This equation represents by a constant temperature ratio the temperature drop of the bleed gas as it passes through the shield. The same constant applies to all three reference points:

$$P_1 = \rho_1 R T_1 \tag{D160}$$

$$\frac{d\rho_{1,E}}{dt} = \frac{1}{V_{1-WT}} (\dot{M}_1 - \dot{M}_{WT}) \tag{D161}$$

$$P_{1,E} = \rho_{1,E} R T_1 \tag{D162}$$

Water-Pump-Turbine Throttle Valve

The mass-flow rate is expressed as

$$\dot{M}_2 = 0.008\, c_{v,2} \frac{P_2}{\sqrt{T_1}} \left[\sqrt{\frac{P_E}{P} - \left(\frac{P_E}{P}\right)^2} \right]_2 \tag{D163}$$

The thermodynamic variables required in this equation are obtained from

$$P_2 = \left(\frac{P_2}{P_1}\right)_{ref} P_1 \tag{D164}$$

$$\frac{d\rho_{2,E}}{dt} = \frac{1}{V_{2-3}} (\dot{M}_{WT} + \dot{M}_2 - \dot{M}_3 - \dot{M}_4) \tag{D165}$$

$$T_{2,E} = T_{3,E} \tag{D166}$$

$$P_{2,E} = \rho_{2,E} R T_{2,E} \tag{D167}$$

Bleed-Pump-Turbine Throttle Valve

The mass-flow rate is

$$\dot{M}_3 = 0.008\, c_{v,3} \left[\frac{P_2}{\sqrt{T_2}} \sqrt{\frac{P_3}{P_2} - \left(\frac{P_3}{P_2}\right)^2}\right]_E \tag{D168}$$

$$\frac{d\rho_{3,E}}{dt} = \frac{1}{V_{3-BT}} (\dot{M}_3 - \dot{M}_{BT}) \tag{D169}$$

$$P_{3,E} = \rho_{3,E} R T_{2,E} \tag{D170}$$

Bleed-Pump-Turbine Bypass Valve

The choked equation applied to this valve is

$$\dot{M}_4 = 0.004\, c_{v,4} \frac{P_4}{\sqrt{T_{2,E}}} \tag{D171}$$

and

$$P_4 = \left(\frac{P_4}{P_{2,E}}\right)_{ref} P_{2,E} \tag{D172}$$

Topping-Turbine Bypass Valve

For this valve, the nonchoked equation is

$$\dot{M}_5 = 0.008\, c_{v,5} \frac{P_{TT,I}}{\sqrt{T_{X,E}}} \left[\sqrt{\frac{P_E}{P_I} - \left(\frac{P_E}{P_I}\right)^2} \right]_{TT} \tag{D173}$$

$$P_{TT,I} = P_{X,E} - K_{TT}\dot{M}_X^2 \tag{D174}$$

The value of K_{TT} was changed to match reference conditions at each of the three sets of bleed-valves positions. The value for $P_{TT,E}$ is obtained from equation (D152).

REACTOR KINETICS

The neutron kinetics is represented by a one-energy group model with six groups of delayed neutrons:

$$\frac{dn}{dt} = \left(\frac{\delta k' - \beta}{l^*}\right) n + \sum_{i'=1}^{6} \lambda_{i'} C_{i'} \tag{D175}$$

where

$$\delta k' = \delta k'_F + \delta k'_w + \delta k'_p \tag{D176}$$

The six equations describing the net rate of formation of the delayed neutron precursors are of the form

$$\frac{dC_{i'}}{dt} = \frac{n\beta_{i'}}{l^*} - \lambda_{i'} C_{i'} \qquad i' = 1,\ 2,\ \ldots\ 6 \tag{D177}$$

The variables in equations (D175) to (D177) are assumed to be independent of space.

A distinctive characteristic of the reactor is the negative temperature reactivity fed back by both the fuel and the water temperatures. The positive contribution to reactivity of the hydrogen density in the core is negligible by comparison.

In the fuel-tungsten mixture a rise in temperature causes the resonance region to be broadened; this phenomenon is known as the neutron Doppler effect. Therefore, more neutrons are absorbed at high energy, which leaves fewer to be thermalized for subse-

quent fission and, thus, reduces the reactivity. The reactivity fed back by the average fuel temperature was expressed as

$$\delta k'_F = -2.67\times10^{-6}\, T_F - 0.01335 \qquad \text{(D178)}$$

The average fuel temperature was approximated by the temperatures of the three axial fuel sections, each weighted approximately according to the reactor-power distribution in its section; that is,

$$T_F = 0.299\, T_{F,A} + 0.339\, T_{F,B} + 0.362\, T_{F,C} \qquad \text{(D179)}$$

The water-temperature reactivity could not be approximated well by a linear function of temperature. Therefore, the variation was set on a variable diode function generator:

$$\delta k'_w = f''(T_w) \qquad \text{(D180)}$$

The average water temperature T_w was determined from the moderator inside and outside water temperatures. The weighting contribution of each was assumed to be proportional to its volume:

$$T_w = 0.2734\, T_{w,i} + 0.7226\, T_{w,o} \qquad \text{(D181)}$$

REFERENCES

1. Chovit, A. R.; and Plebuch, Richard K.: Mission Oriented Advanced Nuclear System Parameters Study. Final Rep. No. STL 8423-`010-RU000, vol. 6 (NASA CR-67317), TRW Space Technology Laboratories, Mar. 1965.

2. Spence, Roderick W.: Nuclear Rockets. Intern. Sci. Tech., no. 43, July 1965, pp. 58-65.

3. Rom, Frank E.; and Ragsdale, Robert G.: Advanced Concepts for Nuclear Propulsion. Nuclear Rocket Propulsion. NASA SP-20, Dec. 1962, pp. 3-15.

4. Lietzke, Armin F.; Saunders, Neal T.; Watson, Gordon K.; Gluyas, Richard E.; and Slaby, Jack G.: Fuel Elements and Fuel-Element Materials, Nuclear Rocket Technology Conference, NASA SP-123, 1966, pp. 217-261.

5. Anon.: Tungsten-Water Moderated Reactor Engine System. Quarterly Progr. Rep., NS 5153-1056, Rocketdyne Div., North American Aviation, Oct. 12, 1965.

6. Anon.: Tungsten-Water Moderated Reactor Engine System. Quarterly Progr. Rep., NA 6153-1017, Rocketdyne Div., North American Aviation, Jan. 25, 1966.

7. Shapiro, Ascher H.: The Dynamics and Thermodynamics of Compressible Fluid Flow. Vol. 1, The Ronald Press Co., 1953.

8. Woods, M. D.; Pierce, B. L.; and Cerni, S.: Hydrogen Properties for Project Nerva. Rep. No. WANL-TNR-043, Westinghouse Astronuclear Lab., Feb. 1962.

9. Miller, John V.; and Taylor, Maynard F.: Improved Method of Predicting Surface Temperatures in Hydrogen-Cooled Nuclear Rocket Reactor at High Surface to Bulk Temperature Ratios. NASA TN D-2594, 1965.

NASA-Langley, 1967 —— 22 E-3439